A Heuristic for Including Black Box Analysis Tools into a Geometric Programming Formulation

by

Cody Jacob Karcher

B.S., Aerospace Engineering, University of Maryland, College Park, 2014

Submitted to the Department of Aeronautics and Astronautics
in partial fulfillment of the requirements for the degree of

Master of Science in Aeronautics and Astronautics

at the

MASSACHUSETTS INSTITUTE OF TECHNOLOGY

May 2017

© Massachusetts Institute of Technology 2017. All rights reserved.

Author .....
Department of Aeronautics and Astronautics
May 25, 2017

Certified by .....
Warren W. Hoburg
Boeing Assistant Professor
Thesis Supervisor

Accepted by .....
Youssef M. Marzouk
Associate Professor of Aeronautics and Astronautics
Chair, Graduate Program Committee

A Heuristic for Including Black Box Analysis Tools into a Geometric Programming Formulation

by

Cody Jacob Karcher

Submitted to the Department of Aeronautics and Astronautics
on May 25, 2017, in partial fulfillment of the
requirements for the degree of
Master of Science in Aeronautics and Astronautics

Abstract

Recently, geometric programming has been proposed as a powerful tool for enhancing aircraft conceptual design. While geometric programming has shown promise in early studies, current formulations preclude the designer from using black box analysis codes which are prolific in the aircraft design community. Previous work has shown the ability to fit data from these black box codes prior to the optimization run, however, this is often a time consuming and computationally expensive process that does not scale well to higher dimensional black boxes. Based upon existing iterative optimization methods, we propose a heuristic for including black box analysis codes in a geometric programming framework by utilizing sequential geometric programming (SGP). We demonstrate a heuristic SGP method and apply it to a solar powered aircraft using a black boxed GP compatible profile drag function. Using this heuristic algorithm, we achieve less than a 1% difference in the objective function between a direct implementation of the constraint and a black box implementation of the constraint.

Thesis Supervisor: Warren W. Hoburg
Title: Boeing Assistant Professor

Acknowledgments

I fully believe that I would not be here without the contributions of many others who helped me and guided me along the way. I would first like to thank my advisor Warren Hoburg for his many contributions and inputs to this work, as well as John Hansman for his guidance and experience. I have also had the great pleasure of working with a number of exceptional and dedicated engineers at Boeing: Bob Liebeck, David Lazzara, Norm Princen, Chris Droney, Sean Wakayama, Jeff Fukushima, and Dean Hawkinson. A special thanks to my family at City on a Hill Church and the Cambridge Community Group for being a constant source of strength and joy. I would also like to thank my various friends with whom grabbing lunch has become regular practice: Cory Frontin, Kevin Archibald, David Miculescu, Devon Jedamski, Sam Schreiner, and Shane Pratt. Thanks also to my friends in the International Center for Air Transportation and the Aerospace Computational Design Laboratory for their ongoing friendship and support. Thanks also to the teaching staff of 16.82x, Tony Tao, Jacquie Thomas, Jennifer Craig and the various student's I have had the pleasure of teaching over the past year. I would also like to thank Albion Bowers and Trevor Gardner, for showing me how to be a godly man while pursuing after scientific discovery. Also to my various teachers from the Grove City Area School District who helped me achieve my goals and played a large part in my academic success. I am indebted to the many University of Maryland and MIT faculty and staff who have helped me become the engineer that I am today, particularly Inderjit Chopra, Raymond Sedwick, Derek Paley, Will Fourney, Aileen Hentz, Mark Drela, Robert Haimes, Ping Lee, Jei Lee Freeman. I would also like to thank my many friends from Team Gamera, particularly Will Staruk and PK Koliais for their friendship and mentorship. Thanks also to my great friends from the MIT Curling Club: Nate Bailey, Alex Hull, Greg Dooley, and Andrea Dubin with whom I have many thoughtful discussions. A special thanks to Kika Arias for her support throughout the writing process. I would most like to thank my parents and brother, Sandra, Victor and Christopher Karcher, for their endless love and support. Finally, to my Heavenly Father, without whom I am nothing.

Contents

1 Importance of Conceptual Design **15**

1.1 The Three-Phase Aircraft Design Process 15

1.2 Conceptual Aircraft Design 17

1.3 Trend of Increasing Design Time 21

2 MDAO in Aircraft Design **23**

2.1 Overview 23

2.2 Definition of a Discipline 24

2.2.1 Performance and Mission Analysis 25

2.2.2 Aerodynamics 26

2.2.3 Propulsion 26

2.2.4 Weights and Structures 26

2.2.5 Stability and Control 27

2.3 Analysis 27

2.3.1 Notion of Fidelity 28

2.3.2 High Fidelity "Black Box" Analyses 30

2.4 Optimization 30

2.4.1 Formulating Mathematical Optimization Problems 31

2.5 Takeaways from MDAO 33

3 Convex Optimization and Geometric Programs **35**

3.1 Convex Optimization 35
3.2 The Geometric Programming Formulation 36
3.3 Geometric Programming for Conceptual Design 38
3.4 Advantages of the Geometric Programming Approach to Conceptual Design 39
3.5 Geometric Programs and Black Boxes 40

4 Iterative Optimization Methods 43
4.1 Sequential Quadratic Programs 43
4.2 Signomial Programs 47
4.3 Sequential Convex Programs 50
4.3.1 Sequential Geometric Programming 51
4.4 General Iterative Methods with Black Boxes 52

5 Proposal for a Heuristic Sequential Geometric Programming Algorithm 53
5.1 Algorithm Introduction 53
5.2 Initialization 54
5.3 Variable Handling 54
5.4 Surrogate Modeling 54
5.5 Black Box Considerations 56
5.6 Creating GP Compatible Constraints 56
5.6.1 Soft-Max Affine (SMA) Functions 56
5.6.2 Number of SMA Terms 57
5.6.3 Interval of Sampling 57
5.6.4 Selecting Points in the Interval 59
5.7 Implementing Trust Regions 59
5.8 Convergence Criteria 60

6 Implementation of the Sequential Geometric Programming Algorithm on a Solar Powered Aircraft 63
6.1 Solar Aircraft Test Problem 63

6.2 User Defined Inputs 65
6.2.1 Initial Guess Values 65
6.2.2 SMA Model Parameters 65
6.2.3 Initial Sampling Interval Parameters 65
6.2.4 Sampling Interval Tightening Parameters 66
6.2.5 Monomial Mode Parameters 66

7 Results of the Sequential Geometric Programming Algorithm 69
7.1 Success Metrics 69
7.2 Algorithm Performance 70

8 Conclusions and Future Work 75
8.1 Summary 75
8.2 Future Work 76
8.2.1 Utilizing Signomial Surrogate Models 76
8.2.2 Implementing New Black Boxes 76
8.2.3 Developing a General SGP Algorithm 77

A Full Report of Design Results 83
A.1 Original Formulation From Burton 83
A.2 Case 1: Hoburg Constraint Implemented as a Geometric Program 93
A.3 Case 2: Hoburg Constraint Implemented as a Sequential Geometric Program 103

List of Figures

1-1 Three phases of aircraft design 16

1-2 Knowledge, cost committed and design freedom in the design process [1] . . 17

1-3 Aircraft concept and experimental airplane 18

1-4 Aircraft concept linking requirements, constraints and objectives [2] (Adapted from [3]) 20

1-5 Increasing development time of modern aircraft [4] 22

2-1 Methods for system decomposition 24

2-2 Aerodynamics fidelity tree 29

3-1 Example of a monomial family 37

3-2 Some posynomial examples 37

4-1 Example optimization problem 45

4-2 The solution of an example sequential quadratic Program 46

4-3 An example signomial program 48

4-4 The solution of an example signomial program 49

4-5 Detailed flowchart of iterative optimization methods 52

5-1 Impact of sampling interval on fit 58

7-1 Convergence of the SGP Algorithm 71

7-2 Impact of changing the initial guess of Case 2 72

7-3 Impact of changing the initial interval of Case 2 73
7-4 Impact of changing the tightening rate of the interval of Case 2 74

List of Tables

7.1 Comparing Solar Aircraft Results 70

Chapter 1

Importance of Conceptual Design

1.1 The Three-Phase Aircraft Design Process

Nevil Shute has a unique position in history as both successful aeronautical engineer and a successful author. In his book *No Highway*, Shute describes the design process from the perspective of a young engineer:

> "A beautiful aircraft is the expression of the genius of a great engineer who is also a great artist. But it is impossible for that man to carry out the whole of the design himself; he works through a design office staffed by a hundred draughtsmen or more. A hundred minds, each with their own ideas, are striving to improve the chief designer's original conception."
>
> -Nevil Shute, *No Highway*

As Shute alludes to, designing a new aircraft can be a massive undertaking, requiring hundreds of engineers, or "draughtsmen," to bring the design from an initial concept to a detailed design that is ready for production. Given the magnitude of this task, aircraft design is typically separated into three phases: conceptual, preliminary and detailed.

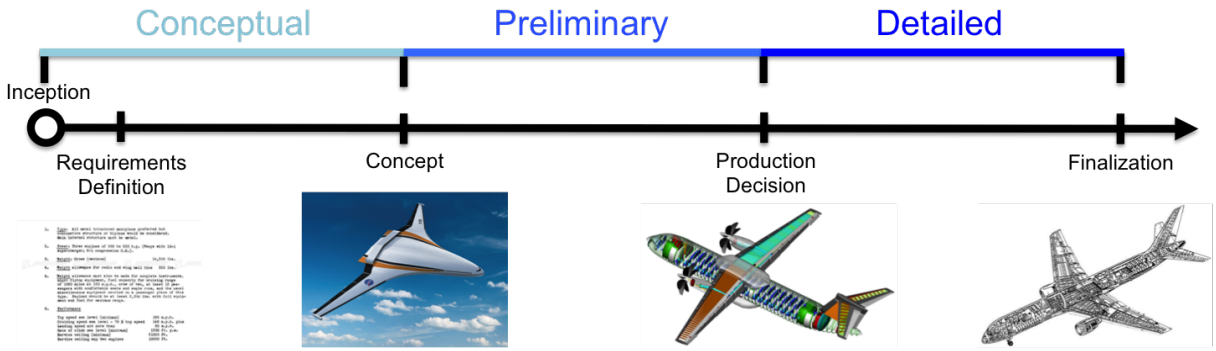

Figure 1-1: Three phases of aircraft design

In most cases, the inception of an aircraft, as indicated in Figure 1-1, and the requirements definition occur simultaneously, and so the purview of conceptual design is to develop a rough geometry and concept of operations from a set of requirements. Conceptual design is fundamentally a creative process [5], linking the function of the concept (the requirements) to the form of the concept (the geometry) [6]. Traditionally, aerodynamics, propulsion, and weights are the disciplines considered in conceptual design.

Preliminary design picks up at the end of conceptual design and brings the aircraft to the point where a production decision will be made. Generally, preliminary design is the phase of the design where 2D geometric representations will be replaced with 3D representations, however, this paradigm has changed in recent years [7, 8]. This 3D geometry then enables high fidelity analysis such as computational fluid dynamics (CFD) and finite element analysis (FEA). Preliminary design traditionally adds stability and control as well as structures to the discipline list. However, as computational tools have become more prolific, the line between conceptual and preliminary design has become less defined, particularly in regard to the classical discipline split.

Detailed design is the final process of creating a production ready design. As Anderson [9] states, detailed design is literally the "nuts and bolts" phase of the design. Transitioning to this phase of the design requires a significant increase in manpower, cost and complexity, and so only the best aircraft designs make it to this phase. Important considerations in

this phase include maintenance, supply chains and ease of manufacture.

Each phase of design has its own unique set of challenges, but conceptual design is perhaps the most crucial for a successful aircraft program. The importance of conceptual design is made apparent by Blanchard and Fabrycky [1]:

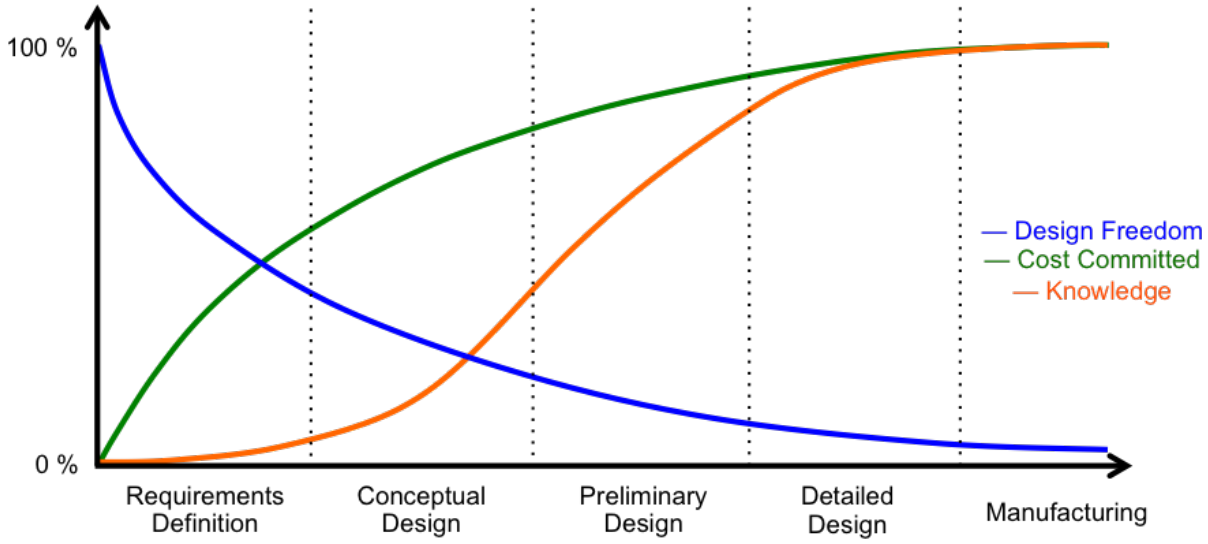

Figure 1-2: Knowledge, cost committed and design freedom in the design process [1]

By the end of conceptual design, decisions have been made that account for a high percentage of the cost and severely limit the design freedom, however the design is still poorly understood until it progresses through the remaining phases of the design process. Given the critical role of conceptual design, this work will primarily focus on this phase.

1.2 Conceptual Aircraft Design

In conceptual design, a designer seeks to develop a concept that is feasible, robust and optimal. Each of these three goals can be captured in a specific question the designer must answer [9]:

1. Feasibility–Is there a concept that meets or exceeds the requirements and constraints?

2. Robustness–How close is the concept to not meeting the requirements and constraints?

3. Optimality–What is the best concept that meets the requirements and constraints?

For an aircraft designer, the term *concept* typically refers to a layout of the major components of the aircraft, along with their relative positions and sizes [9]. Figure 1-3 shows just such a layout, along with the actual experimental aircraft this concept became:

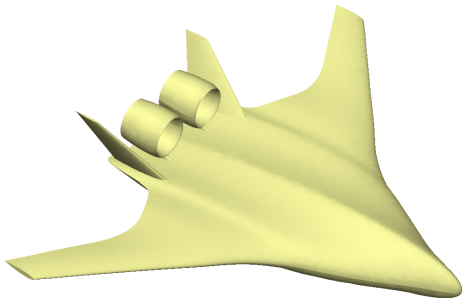

(a) Concept Generated in Engineering Sketch Pad [8]

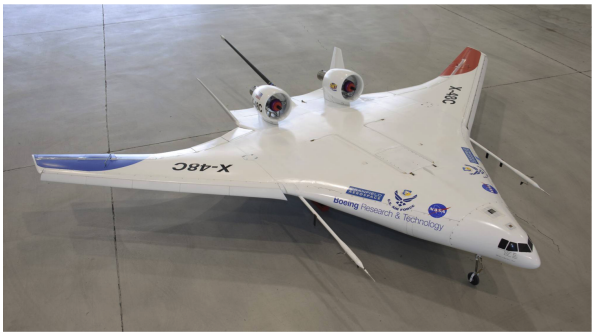

(b) X-48C blended wing body experimental aircraft [10]

Figure 1-3: Aircraft concept and experimental airplane

To generate a concept such as the one in Figure 1-3, a large number of design variables had to be considered, traded and eventually finalized. This set of design variables is frequently referred to as the *design space* for the aircraft concept. Choosing the variables that will make up the design space is often one of the most crucial steps in conceptual design. A poor selection may lead to an intractable optimization problem, while a good selection will capture the features important to the design and create clarity in how the design moves through the design space. Parameters for defining the geometry generally comprise the majority of the space, but performance parameters such as the range of the aircraft, the cruise altitude, or maximum velocity, are also often included as a part of the design space. A general design space could have thousands of dimensions and be infinitely large, but selection of the final concept is governed by three sets of criteria: constraints, objectives and requirements.

Constraints are typically bounds imposed by physics on the design space, for example, the maximum stress in a material cannot be exceeded. A constraint is often treated as a hard cutoff for the design, and is frequently given considerable margin, since exceeding a physical constraint can sometimes have catastrophic consequences.

Objectives are measures of the value or cost of the aircraft, for example, the range the aircraft can fly or the time it takes to manufacture the airplane in the factory. When taken together, these objectives often form an *objective function* which will be maximized or minimized by selecting the correct concept in the design space.

Requirements are the genesis of an aircraft program, typically a list of tasks the aircraft should perform and specifications to which the aircraft is expected to conform. In this way, requirements are a superset of the objectives, with the important distinction that requirements are bounded, while objectives are unbounded. Due to this bounding, system level requirements flow down into secondary subsystem requirements. In practice, requirements are essentially treated as constraints in the design problem, however unlike physical constraints, requirements are often flexible and iterated on between the designer and the customer. This negotiation ensures maximum value is obtained from the new aircraft concept.

The role of the concept is to link together the requirements, constraints and objectives, as shown in Figure 1-4 below.

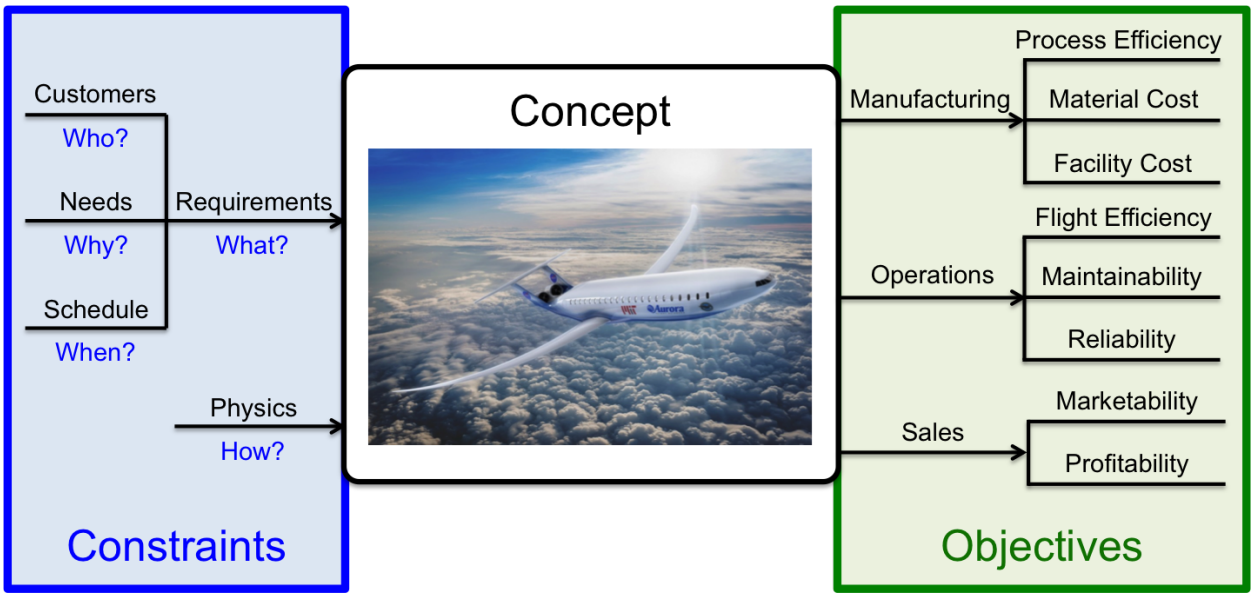

Figure 1-4: Aircraft concept linking requirements, constraints and objectives [2] (Adapted from [3])

Searching a design space is often a daunting task, and the conceptual designer's tool of choice is the trade study. During a trade study, the designer will take a subset of design variables, sweep over the range between some minimum and maximum value, and study the corresponding values of the objectives. This process allows the designer to see how changes in the design variables affect the performance of a concept, providing insight into the best selections for the design variables, along with the sensitivity of the performance of the concept to these selections.

Trade studies have traditionally been performed using empirical or historical methods such as those compiled by Raymer [11], Torenbeek [5], Roskam [12], Shevell [13], Schaufele [14] and Anderson [9], however, advances in high performance computing have altered the landscape in a few ways. First, integrated design tools have enabled trade studies to explore larger design spaces by merging design variables from multiple areas of aircraft design. These tools have relied extensively on the development of Multidisciplinary Analysis and Optimization (MDAO), which will be discussed in Chapter 2. Additionally, physics based analysis methods, which had typically reserved for preliminary and detailed design, have

become available for use in conceptual design. Physics based methods in particular have opened conceptual design to concepts for which no historical or empirical data exists, leading to exciting advances such as the D8 [15] and the blended wing body [16].

1.3 Trend of Increasing Design Time

Despite the role integrated tools and physics based models have played in conceptual design, perhaps the most significant advance in recent years has been the implementation of numerical optimization, enabled by advances in computing technology. Optimization can be used to save the designer time and effort by intelligently searching the space of design variables for the concept which maximizes the objective function, ensuring feasibility, robustness, and optimality.

Numerical optimization has become standard in all aspects of the design community. Tools such as PASS [17], WingMOD [18], SUAVE [19], CEASIOM [20], and TASOPT [21] are just a few examples of tools which have achieved recognition in the aircraft design community. However, despite advances in numerical optimization and increases in computational speed, there is an alarming upward trend in development time for modern aircraft, as shown by Figure 1-5:

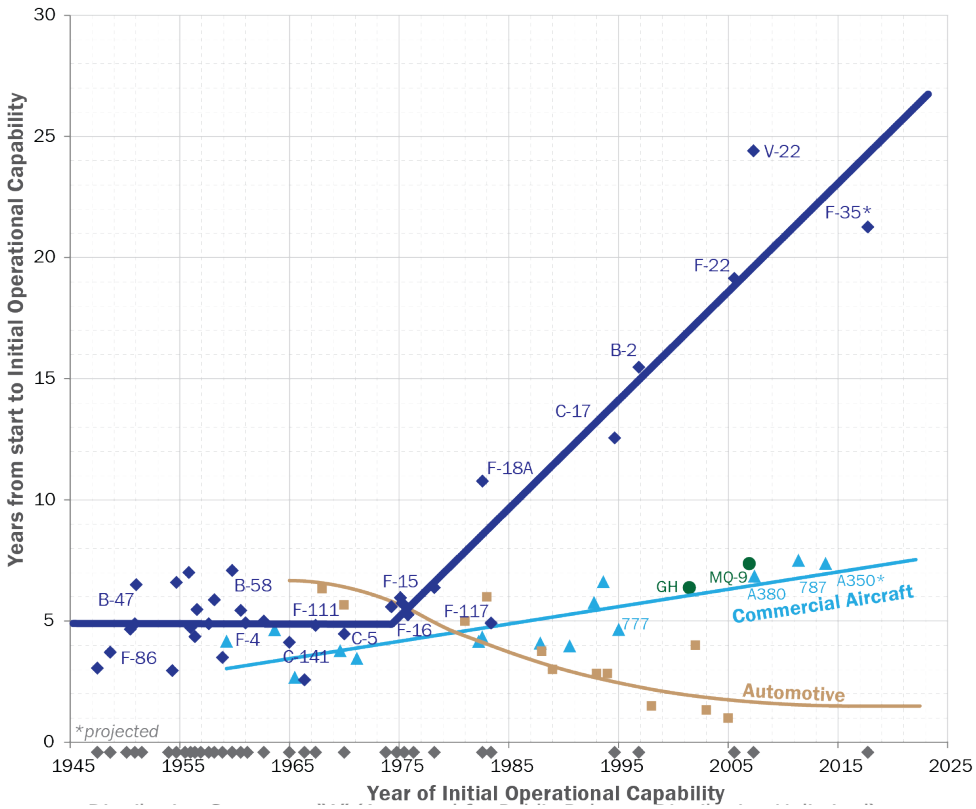

Figure 1-5: Increasing development time of modern aircraft [4]

Simply put, the proliferation of high performance computing does not seem to have resulted in the more rapid development of aircraft. This increasing trend has no single cause and is by no means easy to diagnose, but one major takeaway from this trend is that computational tools must be made as efficient as possible. At time of writing, many tools still can take hours, and in extreme cases weeks or months to run. Thus, the pursuit of efficiency has led to numerous proposals for algorithms, architectures and methods that make the process simpler and more effective. This pursuit is the main goal of the field of Multidisciplinary Analysis and Optimization (MDAO).

Chapter 2

MDAO in Aircraft Design

2.1 Overview

Multidisciplinary Analysis and Optimization (MDAO)[1] is an active field of research focused on the design and optimization of complex systems. Complex system design problems are typically separated into multiple disciplines, or smaller sub-problems, for teams or individuals to address. Individual disciplines have historically been analyzed in isolation, with system level interactions being handled on a case by case basis or via some hierarchy. However, as high performance computation has become more widely available, design teams have been able to consider multiple disciplines simultaneously, giving rise to the field of MDAO. The earliest examples of MDAO came out of attempts to perform coupled aerostructural optimization [22], but it has evolved into a large and diverse field. In this chapter, we will discuss key concepts in MDAO, namely the definition of a discipline, the role of analysis, and methods of optimization.

[1] MDAO is alternatively known as Multidisciplinary Design Optimization (MDO) or simply Multidisciplinary Optimization (MDO)

2.2 Definition of a Discipline

Full scale piloted aircraft can be incredibly complex machines: millions of parts, functioning together in unison. As such, there is no feasible way for a single individual or team to keep track of each detail associated with the airplane. While there are many different ways of decomposing complex systems, two of the most prevalent are physical decomposition and functional decomposition (Figure 2-1).

(a) Physical Decomposition (b) Functional Decomposition

Figure 2-1: Methods for system decomposition

In a physical decomposition[2], components of the aircraft are separated according to their physical location. In contrast, a functional decomposition separates specific tasks on the aircraft and includes all components which address this task. For most aircraft, a functional decomposition is used for the high level systems problem, but physical decompositions tend to be used within functional groups. A functional decomposition also makes the most sense from a project management standpoint, as it is most likely that a subject matter expert in one area will likely be able to apply his or her knowledge to the entire aircraft. One notable exception is aircraft engines, which are typically designed and manufactured by separate companies and then mounted by the airframing company. A functional decomposition leads to the predominant disciplines (or sub tasks) in aircraft design: Aerodynamics, Weights and Structures, Propulsion, Stability and Control, and Performance and Mission Analysis.

While the exact roles of discipline teams can vary widely between organizations, a general breakdown with high level goals and objectives is provided here for the reader. An experienced professional in aircraft design may skip to Section 2.3 without loss of

[2]alternatively a component decomposition

continuity.

2.2.1 Performance and Mission Analysis

The goal of the performance discipline is to compute how well an aircraft performs in the measures defined by the objectives. In this way, performance is the "hub" that ties all of the other disciplines together. Traditionally, the core of the performance discipline has focused on mission analysis, captured best by the Breguet Range Equation[3]:

$$R = \frac{V}{SFC}\frac{L}{D}\ln\left(\frac{W_i}{W_{i+1}}\right) \tag{2.1}$$

which relates several of the major variables of interest. It is immediately apparent how the disciplines tie together: $\frac{VL}{D}$ from aerodynamics, SFC from propulsion, and $\frac{W_i}{W_{i+1}}$ from weights.

While the Breguet Range Equation is incredibly useful for initial sizing, other metrics of classical performance are also of interest, such as takeoff and landing distances, climb performance, and trim. These metrics require a more detailed analysis, leading to a simple mission simulation where the aircraft is treated as a rigid body and simulated over a 2D mission profile, requiring additional data from aerodynamics and propulsion. These higher fidelity calculations enable predictions for those parameters of interest that cannot be captured in the Breguet Range Equation. Eventually, full 6 DOF simulations can be developed using these same principles.

While the focus of the performance discipline has historically been on mission analysis, many aircraft programs are interested in performance metrics beyond flight profiles. Performance metrics such as noise, emissions, observability, maintenance, and

[3]Provided here for jet powered aircraft

manufacturing have become increasingly critical for a wide variety of aircraft programs and will likely receive increased attention in coming years.

2.2.2 Aerodynamics

The aerodynamics discipline is primarily concerned with how the aircraft interacts with the fluid it is traveling through. From the Breguet Range Equation, it is apparent that the main role of the aerodynamics discipline is determining the best $\frac{VL}{D}$ for the aircraft at both nominal and off nominal flight states. However, a secondary objective is to determine the stability and control derivatives over a wide range of flight states. This aero database is necessary for determining control surface effectiveness, trim states, and controllability of the aircraft and typically involves extensive crossover with the Stability and Control discipline.

2.2.3 Propulsion

The propulsion discipline is responsible for all analyses pertaining to the engine. The propulsion discipline must provide an estimate of thrust specific fuel consumption, SFC, which is the weight of fuel consumed per unit of thrust generated in a unit of time. When considering the mission simulation approach to performance, the broader and more useful goal becomes providing engine maps: curves of engine SFC and thrust as a function of throttle setting (or sometimes spool speed), flight speed and altitude.

2.2.4 Weights and Structures

The weights and structures discipline spans all analyses concerning the prediction of the aircraft weight and design of the detailed structural layout. In conceptual design, it is more common to think of this discipline as weight prediction, rather than detailed structures

design, which becomes more prevalent in preliminary and detailed design. While empty weight prediction occupies much of the attention of the weights discipline, an equally vital task is predicting the location of the center of gravity for the aircraft under a variety of loading cases. This CG excursion analysis is crucial for determining both the aerodynamic stability derivatives and the trim state the airplane, which can significantly impact performance.

2.2.5 Stability and Control

The stability and control (S&C) group is primarily responsible for sizing the aircraft empennange and control surfaces, working in conjunction with the aerodynamics group. An additional function of the S&C group is to provide the first high level control scheme that will eventually be perfected in a flight control system during the detailed design process. This responsibility includes sizing control actuators, along with predicting dynamic performance of the aircraft, and performing eigenmode analysis.

2.3 Analysis

As was alluded to in the discussion of each of the disciplines, a discipline will typically receive a set of inputs from the system problem and then provide a set of outputs back. The mathematical mapping from inputs to outputs is referred to as *analysis*. The field of analysis is exceedingly complex, having multiple levels and requiring advanced understanding of the discipline in question. In addition, the analysis step is the most expensive step by far in terms of cost, manpower and time.

2.3.1 Notion of Fidelity

Each discipline group in aircraft design has a number of tools at their disposal. For example, an aerodynamics team might have a wide variety of analytical and testing options including basic aerodynamic analysis, various computational methods, or flight testing. Any one of these options will produce the required data (or outputs to the systems problem), however, some of these methods will be trusted to provide a more accurate number as compared to physical reality than others. This degree of accuracy is often referred to as the "fidelity" of the analysis method, however it may also be referred to as the "order" of the analysis. Increasing fidelity results in a higher degree of confidence (less uncertainty) in the final result, but at the cost of increased expense, either computationally or monetarily. These analysis methods can be organized into a so-called "fidelity tree" (Figure 2-2)[4], shown here for the Aerodynamics discipline.

[4]While most designers or design groups hold to this type of tree, the methods are rarely written in order of trust like this, as trust in a tool or method will be highly dependent on personal experience

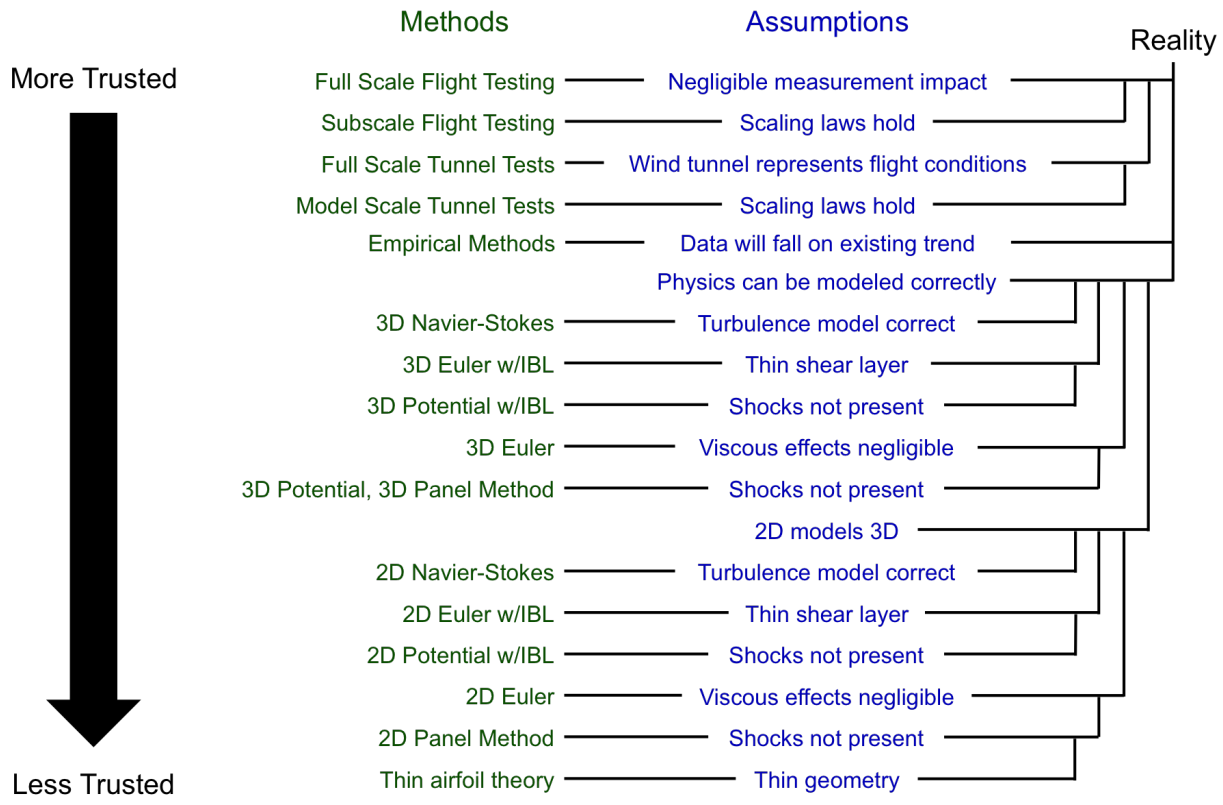

Figure 2-2: Aerodynamics fidelity tree

This tree describes the assumptions that must be made to "trust" the result from an analysis method, with each assumption moving the method further away from the true physics of the problem. Assumptions go down the middle of the tree, with the analysis methods listed on the left hand side. As an example, only one assumption is required on this fidelity tree to reach full scale flight test, but five assumptions are required to reach Thin Airfoil Theory, meaning that in general, the data from flight testing is considered more trustworthy than the predictions from Thin Airfoil Theory. This particular tree has been set up such that methods at the top of the tree are generally considered to be more "trusted", and therefore of higher fidelity than tools lower on the chart. Fidelity trees can be set up for any discipline, but a survey is beyond scope here. Price [23] provides a "Nickol chart" which is a compilation of these fidelity trees for a variety of disciplines.

2.3.2 High Fidelity "Black Box" Analyses

In practice, each branch of a fidelity tree corresponds to a different tool or method that the discipline team is capable of utilizing. Testing is often too expensive to be practical for development and is therefore reserved for validation. Thus, computational methods dominate conceptual design, and a wide variety of these methods are available depending on the application. For example, when a 2D full potential code with an integrated boundary layer correction is required, XFOIL is commonly used, whereas 3D viscous flow will require a CFD code like OVERFLOW. Writing an analysis tool or method is a large undertaking, requiring detailed expertise and coming at the price of a large development cost. As a result, the tendency is to treat an existing method as a "black box". The term "black box" refers to the fact that the user is unaware of the inner workings of the analysis code, but can simply be trained on how to feed in inputs and interpret outputs. These black boxes are prolific in the aircraft industry across all disciplines and, at the time of this writing, are critical components of all three phases of the design process. In fact, many black box codes used to this day are decades old legacy codes that are highly trusted and would be costly to replace. Thus, a major focus of the MDAO community has been studying how to make these discipline black boxes communicate with each other in the most effective way possible for the purposes of design and optimization. Many of these approaches are outlined by Martins and Lambe [22], but a full discussion of MDAO methods is beyond scope here.

2.4 Optimization

To this point, all that has been discussed is the *analysis* element of the design process. In other words, if a design is reached, it can be fed into these cascading analyses and a performance evaluation can be output. A designer must close this loop, taking the performance outputs and using them to inform changes in the design. As was stated in

Chapter 1, the set of design variables that collectively describe the aircraft design is often referred to as the *design space* of the aircraft. The greatest challenge for the designer is deciding which design in this design space is the best one, and in this pursuit, the designer's most powerful tool is optimization. At its best, optimization can be thought of as a series of automated and simultaneous trade studies, capable of evaluating multiple trades and arriving at the best design. In practice, optimization falls well short of this goal, but is still incredibly useful in finding the "best" design near a designer's informed guess, determining the ways in which the designer should manipulate the current design, and guiding the designer away from dangerous regions in the design space.

2.4.1 Formulating Mathematical Optimization Problems

Chapter 1 discussed the role optimization plays in the aircraft design process, but how does one turn aircraft design into a mathematical optimization problem? The first step is to write an objective function, which generally serves as a surrogate for the value of the aircraft being designed.[5] Example objective functions are as follows:

$$\begin{gathered} W_{MTO} \\ \frac{SFC}{V}\frac{1}{L/D} \\ N_{eng}W_{engine} + W_{fuselage} + W_{wing} + W_{avionics} + W_{empennage} \end{gathered} \tag{2.2}$$

Additionally, constraint functions are written which bound the space of feasible solutions. As discussed in Chapter 1, constraints can come from underlying physics or from imposed requirements. In numerical optimization, constraints take the form of equalities and

[5] A more detailed discussion of aircraft objectives is located in Chapter 1

inequalities, such as the following:

$$\begin{aligned} L &= \frac{1}{2}\rho V^2 C_L S \\ \sigma_{y_{\text{Al}}} &\leq 55 \text{ MPa} \end{aligned} \tag{2.3}$$

With these two concepts of mathematical objectives and constraints, we can introduce the form of a mathematical optimization problem [24]:

$$\begin{aligned} &\text{minimize} && f_0(\mathbf{x}) \\ &\text{subject to} && f_i(\mathbf{x}) \leq b_i,\ i = 1, \ldots, m \end{aligned} \tag{2.4}$$

where f_0 is the objective function and the f_i are the constraints which are constrained to be less than or equal to a constant b_i[6]. A simple example of minimizing the drag of a wing

[6]Note that any inequality can be manipulated into this form

is as follows [25]:

$$
\begin{aligned}
\text{minimize} \quad & D \\
\text{subject to} \quad & C_{D_{fuse}} = \frac{(CDA0)}{S} \\
& C_{D_{ind}} = \frac{C_L^2}{A\pi e} \\
& Re \leq \frac{\rho V}{\mu}\left(\frac{S}{A}\right)^{0.5} \\
& C_f \geq \frac{0.074}{Re^{0.2}} \\
& C_{D_p} = \left(\frac{S}{S_{wet}}\right) C_f k \\
& C_D \geq C_{D_p} + C_{D_{fuse}} + C_{D_{ind}} \\
& W_w \geq S W_{W_{coeff2}} + \frac{A^{1.5} N_{ult} S^{0.5} W^{0.5} W_0^{0.5} W_{W_{coeff1}}}{\tau} \\
& W \leq \frac{1}{2}\rho V^2 C_L S \\
& W \leq \frac{1}{2}\rho V_{min}^2 C_{L,max} S \\
& W \geq W_0 + W_w \\
& D \geq \frac{1}{2}\rho V^2 C_D S
\end{aligned}
\tag{2.5}
$$

2.5 Takeaways from MDAO

MDAO represents the state of the art of aircraft design, and in fact all complex system design. It is therefore crucial that any design or optimization work understand the main takeaways from this community. First, black box analysis codes are critical to real system design. The development cost and time that is required to develop new methods is simply too high for practicing design teams. Second, and perhaps more crucial here, is the fact that a vast majority of MDAO takes an analysis first approach, focusing on intelligent ways to wire the black box codes together into large analysis codes, and then complex optimization algorithms are used to solve the problem. However, a recent development is

the optimization first approach taken by Hoburg [25]. His proposal is that rather than focus on the analysis, emphasis should be placed on highly efficient optimization, for example Geometric Programs (GPs), and analysis methods should be integrated into this highly efficient framework. The geometric programming approach will be introduced in the next chapter.

Chapter 3

Convex Optimization and Geometric Programs

3.1 Convex Optimization

Hoburg [25] has recently proposed a paradigm shift in conceptual design, that efficient optimization be utilized and models developed to fit this new optimization framework. At the core of this proposal is the notion of convex optimization. Floudas [26] defines the notion of convexity using Jensen's Inequality:

$$f[(1-\lambda)\mathbf{x}_1 + \lambda\mathbf{x}_2] \leq (1-\lambda)f(\mathbf{x}_1) + \lambda f(\mathbf{x}_2) \tag{3.1}$$

As a result of this mathematical property, convex optimizations can be solved quickly and efficiently. A convex optimization problem as defined by Boyd [24] is one where the objective and constraint functions are convex. By sticking to this form, we obtain a number of benefits over a general non-linear programs (NLPs). First, NLPs make no guarantees on global optimality, where as the Jensen Inequality ensures that any optimum

of a convex function is global. Second, convex optimization problems do not require initial guesses to converge to the global optimum as any initial guess is guaranteed to converge to the optimum. Finally, convex optimization problems can be solved very rapidly utilizing interior point methods [24].

Despite the many advantages of convex optimization, a potential drawback is that, by definition, all objectives and constraints must be convex. However, work pioneered by Hoburg [25] has demonstrated that by utilizing a geometric programming formulation, this is not a serious limitation in the case of aircraft conceptual design through the use of Geometric Programming (GP).

3.2 The Geometric Programming Formulation

A geometric program (GP) is an optimization problem that is convex when transformed into logspace [27]. In order for this condition to be true, the objectives and constraints must take a special form, specifically that of a monomial or posynomial function. A monomial function takes the form:

$$f(\mathbf{x}) = c{x_1}^{a_1}{x_2}^{a_2}... \ {x_n}^{a_n} \tag{3.2}$$

where $\mathbf{x}$ is a vector of n decision variables, c is a positive scalar, and the exponents a_i are real numbers. A family of monomials ($c = 1$) is plotted below (Figure 3-2), along with the transformation to logspace.

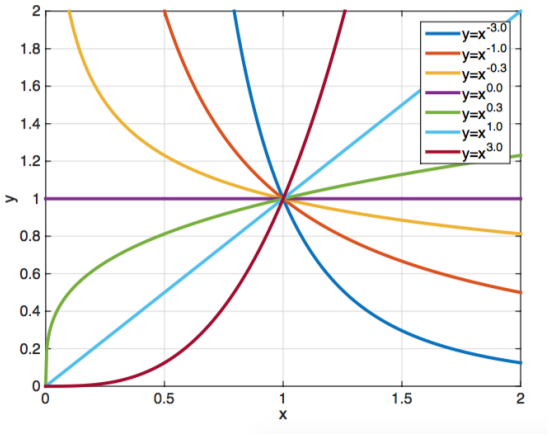

(a) Monomials in standard coordinates

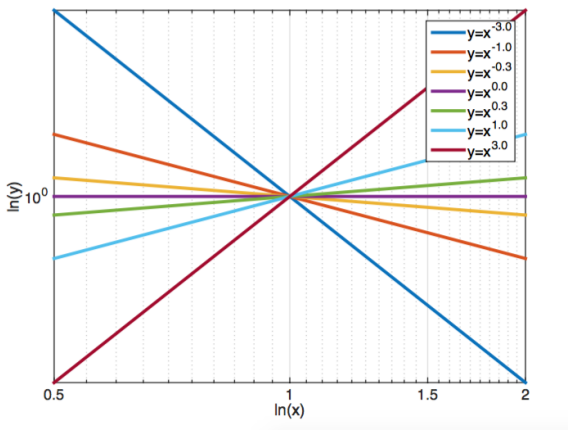

(b) Monomials transformed into logspace

Figure 3-1: Example of a monomial family

Note that all monomial functions become *affine* or *linear* upon transformation, meaning that any function that can be written in monomial form can be converted into an affine function in logspace. A posynomial is then defined as the sum of one or more monomial functions:

$$g(\mathbf{x}) = \sum_{k=1}^{K} c{x_1}^{a_{1k}} {x_2}^{a_{2k}} \ldots {x_n}^{a_{nk}} \tag{3.3}$$

Given this form, a few examples are plotted below:

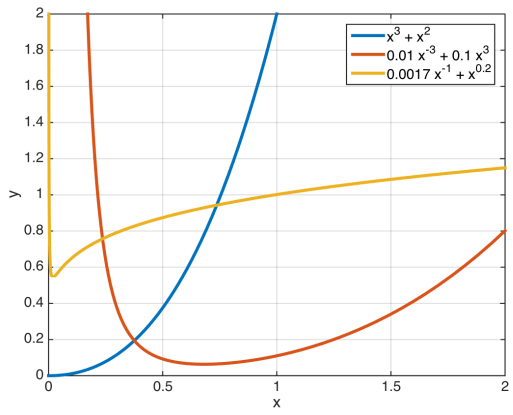

(a) Posynomials in standard coordinates

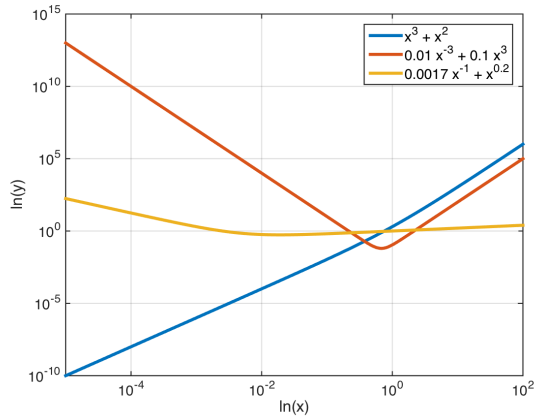

(b) Posynomials transformed into logspace

Figure 3-2: Some posynomial examples

Note that posynomials need not be convex in regular space, but after transformation do indeed become convex. Therefore, any set of objectives that can be written as monomials and posynomals is *convex* in logspace. With these definitions, we can define the standard form of a GP [27]:

$$\begin{aligned} &\text{minimize} && g_0(\mathbf{x}) \\ &\text{subject to} && f_i(\mathbf{x}) = 1,\ i = 1, \ldots, m \\ & && g_i(\mathbf{x}) \leq 1,\ i = 1, \ldots, p \end{aligned} \tag{3.4}$$

where f_i are monomial functions and g_i are posynomial functions. Boyd [27] provides the following example GP:

$$\begin{aligned} &\text{minimize} && x^{-1}y^{-1/2}z^{-1} + 2.3xz + 4xyz \\ &\text{subject to} && (1/3)x^{-2}y^{-2} + (4/3)y^{1/2}z^{-1} \leq 1 \\ & && x + 2y + 3z \leq 1 \\ & && (1/2)xy = 1 \end{aligned} \tag{3.5}$$

When a problem is written in this form, we say that it is *GP compatible* and can be solved by commercial off the shelf codes.

3.3 Geometric Programming for Conceptual Design

Hoburg's [25] breakthrough was that many problems of interest to the aircraft design community fit into this monomial and posynomial form. By reviewing Equation 2.5, this

becomes evident:

$$
\begin{aligned}
\text{minimize} \quad & \frac{1}{2}\rho V^2 C_D S \\
\text{subject to} \quad & 1 \geq \frac{0.074}{C_f Re^{0.2}} \\
& 1 \geq \frac{(CDA_0)}{C_D S} + \frac{kC_f S_{wet}}{C_D S} + \frac{C_L^2}{C_D \pi e AR} \\
& 1 \geq \frac{2W}{\rho V^2 C_L S} \\
& 1 \geq \frac{W_0}{W} + \frac{W_w}{W} \\
& 1 \geq 45.42\frac{S}{W_w} + 8.71 \times 10^{-5}\frac{N_{lift} A^{3/2}\sqrt{W_0 W S}}{W_w \tau} \\
& 1 \geq \frac{2W}{\rho V_{min}^2 C_{L_{max}} S} \\
& 1 = \frac{\rho V}{\mu Re}\sqrt{\frac{S}{A}}
\end{aligned}
\tag{3.6}
$$

Hoburg goes on to develop models for propulsion, loads, structures, and aerodynamics. Using the GP formulation, Hoburg demonstrated the ability to perform conceptual design of aircraft in fractions of a second, significantly expanding the ability of the designer to study the design space.

3.4 Advantages of the Geometric Programming Approach to Conceptual Design

Many advantages come from taking a geometric programming approach to aircraft design. First, the mathematics of conceptual design tend to be GP compatible, which is convenient to implement. Second, since objectives and constraints take the same form (monomial and posynomial) requirements can quickly be swapped out as either the objective of the optimization or a constraint in the problem. Third, since GP is a convex formulation,

designs are arrived at rapidly and guarantee global optimality. In the context of MDAO, GP has an additional advantage. GP is referred to as a Simultaneous Analysis and Design (SAND) architecture. SAND architectures are the least expensive computationally [28] and are therefore are attractive for conceptual design, but a SAND approach requires that all discipline analysis equations be treated explicitly as constraints in the formulation [22], requiring a great deal of effort on the part of the designer to implement. GP keeps the computational benefit of a SAND architecture, and since most equations of interest are directly GP compatible, the impracticality of implementation is significantly reduced. In fact, by utilizing GPkit [29], implementation of a GP is as simple as transcribing the equations of interest.

3.5 Geometric Programs and Black Boxes

As was discussed in Chapter 2, black boxed analysis codes play a critical role in the design process, and therefore a key drawback of the GP formulation is the exclusion of these black boxes. There is no way for a GP to solve with a constraint that is not GP compatible, and thus to incorporate a general black box, one of three approaches must be taken. First, all of the mathematics of the black box can be rewritten into a GP compatible analysis code and implemented directly as constraints in the GP formulation. This method works well for small problems and low fidelity analyses, however quickly becomes impractical. In addition, many analysis, such as high fidelity aerodynamics, are inherently not GP compatible and could not be implemented in this form.

Second, the black box can be pre-sampled and fit with an explicit GP compatible mathematical function. This is the approach taken by Hoburg [30], enabled by GPfit [31]. This approach solves the key problem in a direct implementation approach in that the mathematics of the black box itself do not have to be convex, only the relation between inputs and outputs. For example, this relationship tends to hold true for relationships

between C_L and C_D, but the mathematics required to estimate a C_D for a given C_L are not inherently GP compatible beyond the lowest levels of fidelity. The limit to this approach is the number of design variables considered by the black box, as the computational time to sweep over the black box increases with the number of inputs to the black box (unless parallelization is available). This limitation makes this approach challenging, perhaps even infeasible, for black boxes with many inputs and outputs.

Finally, an iterative optimization algorithm can be implemented where the black box analysis is called as the algorithm iterates. This approach sacrifices the guarantees inherited from the GP, including rapid convergence and global optimality, but provides the most flexibility, enabling general black box integration without the curse of dimensionality that arises when pre-computing all the data. To further investigate this idea, inspiration is drawn from existing iterative optimization methods that will be discussed in Chapter 4.

Chapter 4

Iterative Optimization Methods

4.1 Sequential Quadratic Programs

The primary issue raised in Chapter 3 is that the GP formulation does not naturally lend itself to the use of black box analyses. However, in the past, iterative optimization algorithms have been utilized in order to incorporate black boxes, with sequential quadratic programs (SQPs) being among the most common in the aircraft design community [17, 32], due to their effectiveness, simplicity, and flexibility. A sequential quadratic program is a generic non-linear solution algorithm that approximates the design space as a quadratic program (QP) local to the current design point, and then iterates until convergence is reached.

A quadratic program (QP) takes the form [33]:

$$\begin{aligned} \text{minimize} \quad & q(x) = \frac{1}{2}x^T G x + x^T c \\ \text{subject to} \quad & a_i^T x = b_i, \qquad i \,\epsilon\, \mathcal{E} \\ & a_i^T x \geq b_i, \qquad i \,\epsilon\, \mathcal{I} \end{aligned} \tag{4.1}$$

Note here that the objective is a quadratic function of x, and the constraints are linear in x.

Considering sequential quadratic programs, we seek to solve the generic non-linear optimization problem, or non-linear program (NLP) [34]:

$$\begin{aligned} \text{minimize} \quad & f(\mathbf{x}) \\ \text{subject to} \quad & h(\mathbf{x}) = 0 \\ & g(\mathbf{x}) \leq 0 \end{aligned} \tag{4.2}$$

For an SQP algorithm, we take our current design vector $\mathbf{x}^k$ and approximate the optimization problem locally as a quadratic program [34]:

$$\begin{aligned} \text{minimize} \quad & \nabla f(\mathbf{x}^k)^T d_x + \frac{1}{2} d_x^T \nabla^2 f(\mathbf{x}^k) d_x \\ \text{subject to} \quad & \nabla h(\mathbf{x}^k)^T d_x + h(\mathbf{x}^k) = 0 \\ & \nabla g(\mathbf{x}^k)^T d_x + g(\mathbf{x}^k) \leq 0 \\ & d_k = \mathbf{x} - \mathbf{x}^k \end{aligned} \tag{4.3}$$

The SQP algorithm takes the first and second derivatives of the objective and fits the objective locally with a quadratic function. Additionally, the first derivative is taken of all of the constraints, and a local linear fit is performed. This forces the general non-linear program into a QP formulation. Consider the following example:

$$\begin{aligned} \text{minimize} \quad & 100x^{0.8}y^{0.8} + 10x^{0.8}y^{-0.8} + 10y^{0.8}x^{-0.8} + x^{-0.8}y^{-0.8} \\ \text{subject to} \quad & 8xy - 1 = 0 \\ & 1.1x + 0.2 - (x^2 + y) \leq 0 \end{aligned} \tag{4.4}$$

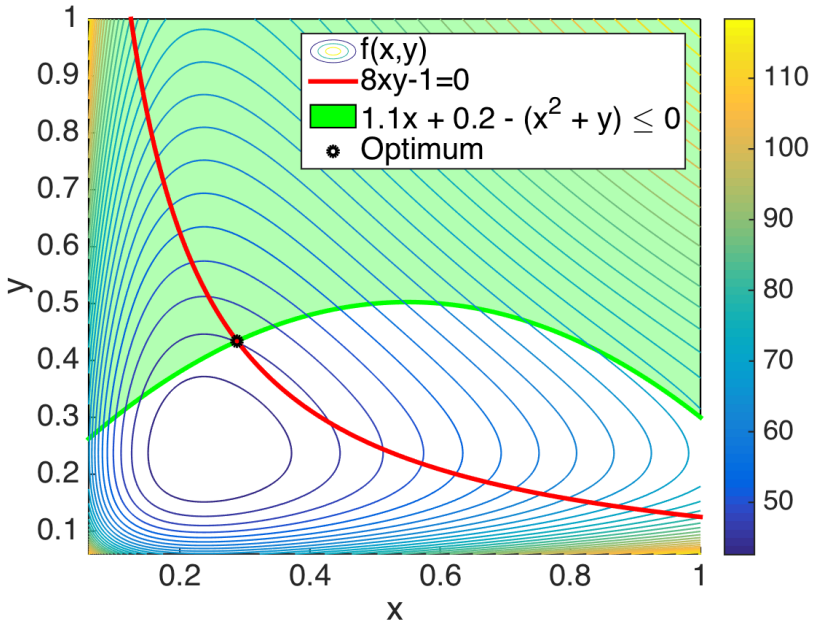

Figure 4-1: Example optimization problem

Applying the SQP algorithm, a graphical solution can be compiled:

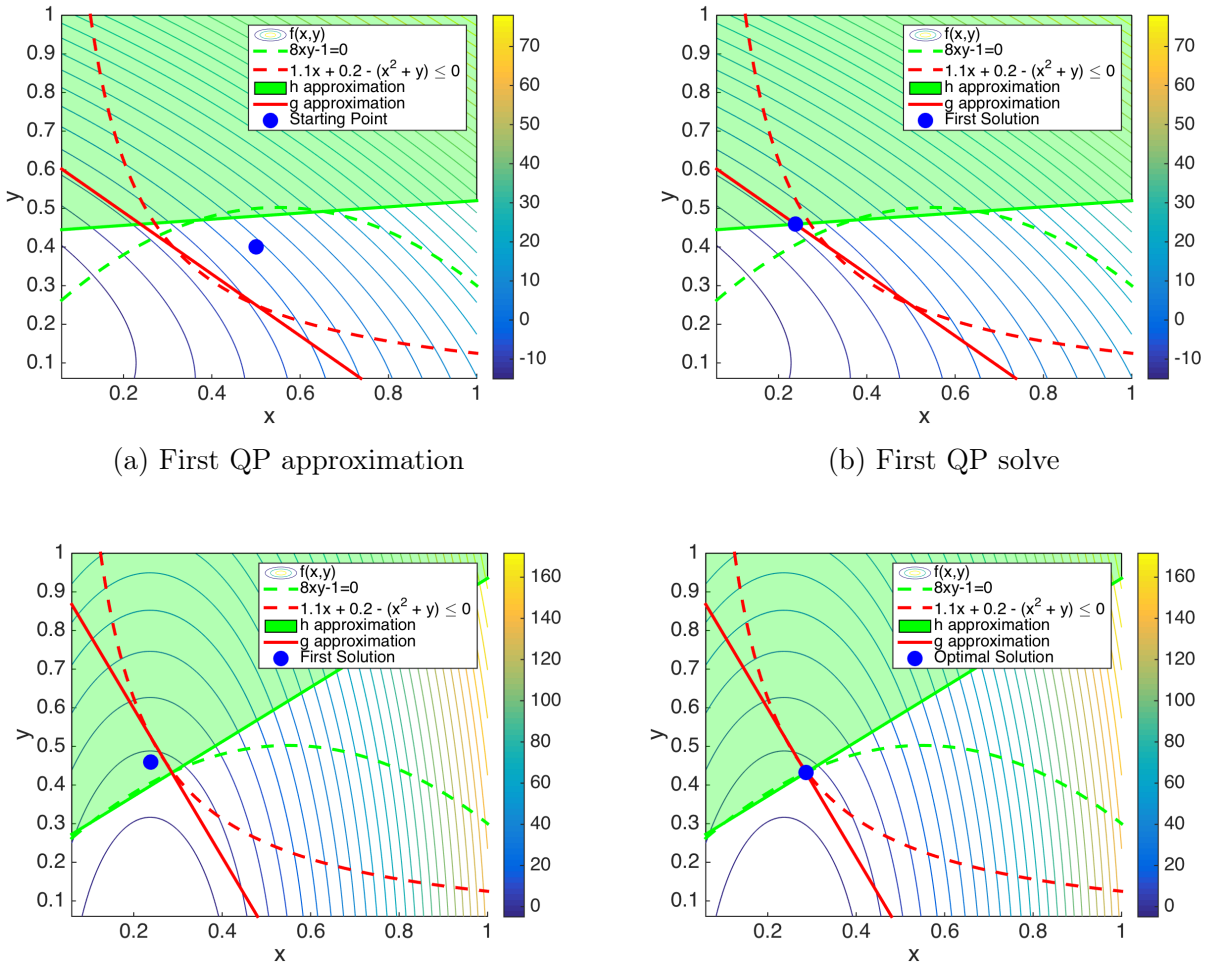

(a) First QP approximation

(b) First QP solve

(c) Second QP approximation

(d) Final QP solve

Figure 4-2: The solution of an example sequential quadratic Program

With this algorithm, the objective and constraints are approximated in a QP form that can be solved rapidly by the optimizer. As the algorithm progresses, the approximation becomes closer to the actual underlying mathematics until convergence to a relative tolerance.

The linear form of the constraints in each QP subproblem provides an avenue for incorporating the black box analyses. A linear constraint can be computed for each black box using the derivatives of the output variables with respect to the input variables. These derivatives can be obtained by using finite-differencing, adjoint methods or some other

differentiation scheme, and hence the penalty of calculating the linear constraints equivalent to the penalty of computing the derivatives. But despite the versatility of the SQP algorithm, it does not take full advantage of the GP formulation, and so another approach should be considered.

4.2 Signomial Programs

A signomial program (SP) is a geometric program which has been modified to include subtraction of terms. By a rigorous definition, a signomial is defined as the linear combination of monomial terms [24]. By this definition, we can also write a signomial as the difference between two posynomials:

$$h(\mathbf{x}) = \sum_{k=1}^{K} c {x_1}^{a_{1k}} {x_2}^{a_{2k}} \ldots {x_n}^{a_{nk}} - \sum_{l=1}^{L} d {x_1}^{a_{1l}} {x_2}^{a_{2l}} \ldots {x_n}^{a_{nl}} \tag{4.5}$$

A signomial program in standard form can then be defined:[24, 35]

$$\begin{aligned} \text{minimize} \quad & \frac{p_0(\mathbf{x})}{p_1(\mathbf{x})} \\ \text{subject to} \quad & h_i(\mathbf{x}) = 0, \ i = 1, \ldots, m \\ & h_j(\mathbf{x}) \leq 0, \ j = 1, \ldots, p \end{aligned} \tag{4.6}$$

By using the SP formulation, many of the same mathematical advantages of the GP formulation are maintained and the ability to subtract terms in the constraints is also available. The extensibility of the SP formulation to aircraft design has been demonstrated by Kirschen [36]. While SPs can accommodate a broader range of models, they lose all of the guarantees that can be made by GPs due to the non-convexity introduced by the subtraction, however, of interest here is the SP solution method. Consider the same

example from above, but this time plotted in logspace:

$$\begin{aligned} \text{minimize} \quad & 100x^{0.8}y^{0.8} + 10x^{0.8}y^{-0.8} + 10y^{0.8}x^{-0.8} + x^{-0.8}y^{-0.8} \\ \text{subject to} \quad & 8xy - 1 = 0 \\ & 1.1x + 0.2 - (x^2 + y) \leq 0 \end{aligned} \tag{4.7}$$

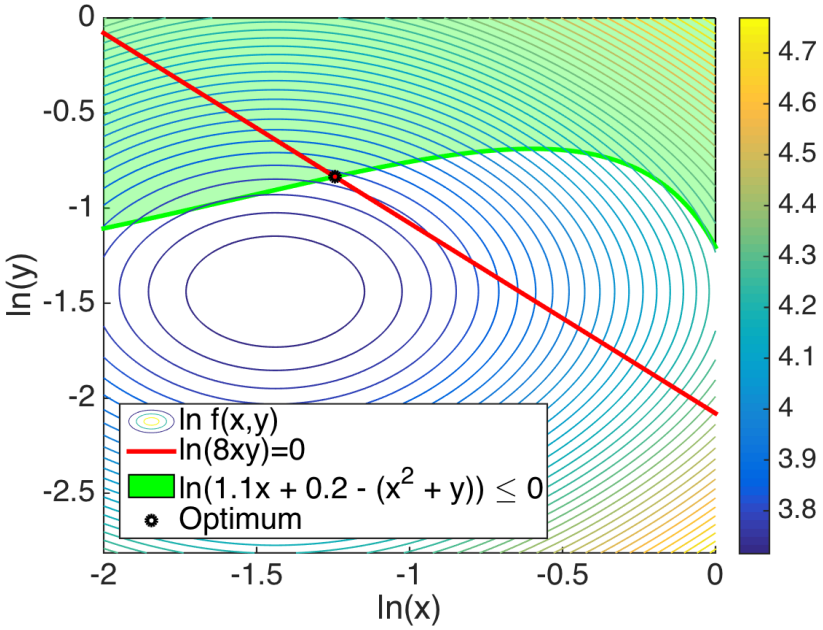

Figure 4-3: An example signomial program

As we can see in Figure 4-3, we have introduced a constraint which is concave in logspace. Now, the best possible GP compatible fit we can make to this constraint is affine in logspace. So, we select an initial point and make this approximation. This GP is then solved, creating a new design point. The linearizion and solving process is then repeated until a certain relative tolerance is achieved. The solution process is shown below in Figure 4-4:

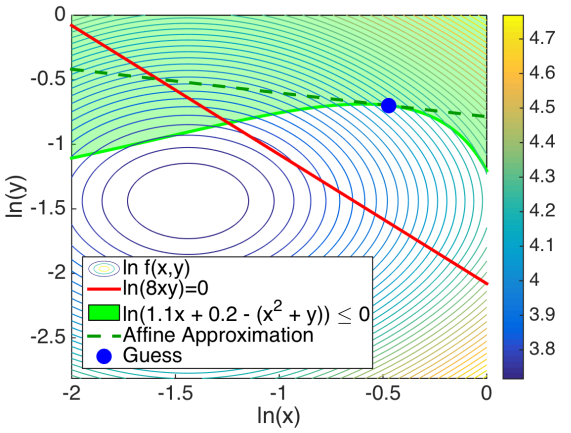

(a) Initial linearization

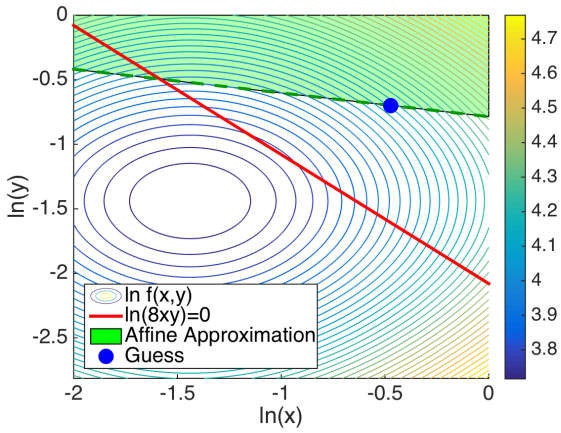

(b) Formulating the GP

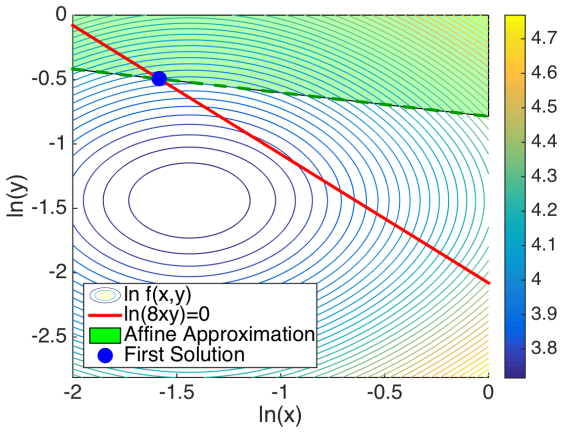

(c) Solving the first GP

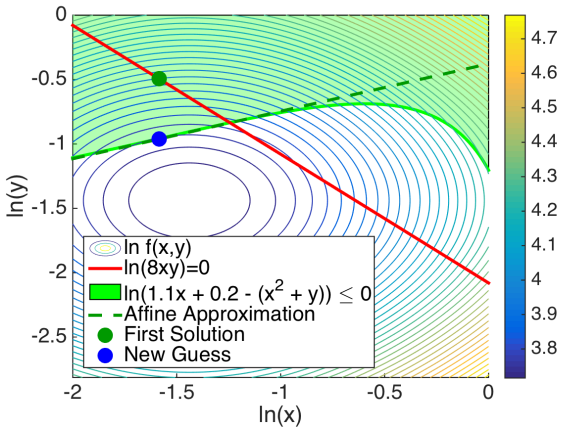

(d) Updating to a new GP

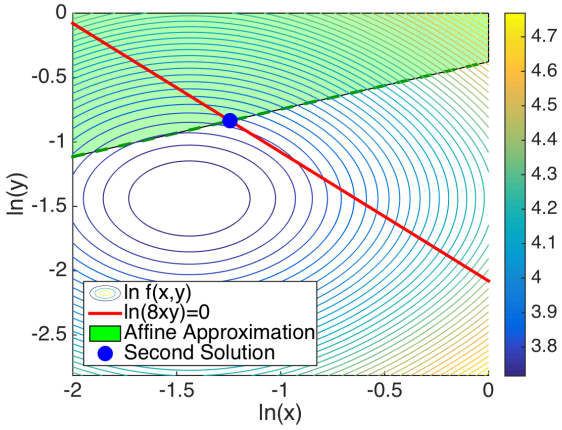

(e) Solving the new GP

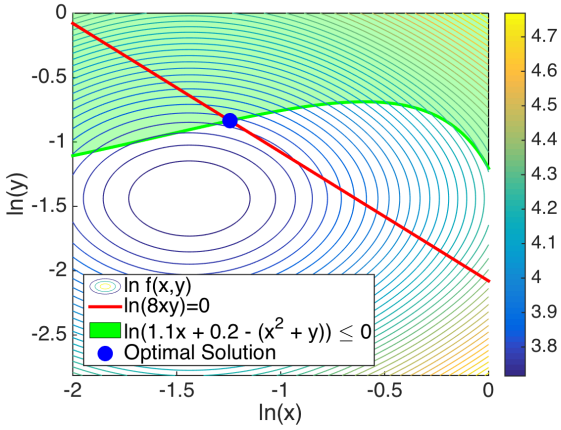

(f) Converged to final solution

Figure 4-4: The solution of an example signomial program

Signomial programs provide us with an important perspective, demonstrating how geometric programs can be used in an iterative fashion to solve problems which are not GP compatible. However, unlike SQP, there is no longer a convenient way of incorporating black boxes, as the solution algorithm still requires explicit signomial constraints which can be relaxed. Thus, we must take the black box functionality of SQP along with the GP core of SP.

4.3 Sequential Convex Programs

Boyd [37] outlines methods for solving a sequence of convex problems. While the SQP algorithm is one example of a sequential convex program (SCP), Boyd primarily discusses the Difference of Convex Programming (DOC) algorithm. A DOC is a superset of signommial programming (SP), where the optimization problem takes the form:

$$\begin{aligned} &\text{minimize} && f_0(\mathbf{x}) - g_0(\mathbf{x}) \\ &\text{subject to} && f_i(\mathbf{x}) - g_i(\mathbf{x}) \leq 0,\ i = 1, \ldots, m \end{aligned} \tag{4.8}$$

where f_i and g_i are both convex functions. Difference of convex programs are typically solved using the Convex-Concave Procedure (CCP), where the concave functions g_i are approximated as linear by [38]:

$$\hat{g}_i(\mathbf{x}; \mathbf{x}_k) = g_i(\mathbf{x}_k) + \nabla g_i(\mathbf{x}_k)^T(\mathbf{x} - \mathbf{x}_k) \tag{4.9}$$

and then a single iteration becomes:

$$\begin{aligned} &\text{minimize} && f_0(\mathbf{x}) - \Big(g_0(\mathbf{x}_k) + \nabla g_0(\mathbf{x}_k)^T(\mathbf{x} - \mathbf{x}_k) \Big) \\ &\text{subject to} && f_i(\mathbf{x}) - \Big(g_i(\mathbf{x}_k) + \nabla g_i(\mathbf{x}_k)^T(\mathbf{x} - \mathbf{x}_k) \Big) \leq 0,\ i = 1, \ldots, m \end{aligned} \tag{4.10}$$

which we can now guarantee will be a convex problem. This guarantee can be made because any strictly convex function f_i in linear combination with a linear (or quasi-convex) function $\hat{g}_i(\mathbf{x}; \mathbf{x}_k)$ will also be convex [26]. The sub-problem then inherits the various benefits associated with convexity.

Studying the CCP algorithm helps us identify key areas in which general SCP algorithms can be advantageous over SQP algorithms. As discussed by Lipp and Boyd [38], the CCP retains more information about the underlying mathematics of the original problem in each subproblem, especially in the constraints. While the constraints in an SQP must be linear, the constraints in a CCP solve are limited only to be convex and hence contain second derivative information. Additionally, the linear approximation of the concave portion of the problem ensures that this linear approximation is a global overestimation, thus the trust regions that are sometimes required in SQP are are not necessary.

4.3.1 Sequential Geometric Programming

The term sequential geometric programming (SGP) appears very little in the literature, save one paper [39], and does not seem to have gained widespread acceptance nor developed a standard definition. We define a sequential geometric programming algorithm as a solution method for non-linear programs (NLPs) where several geometric programming approximations are solved sequentially. An SGP algorithm solves the following NLP:

$$\begin{aligned} \text{minimize} \quad & g_0(\mathbf{x}) \\ \text{subject to} \quad & f_i(\mathbf{x}) = 1, \ i = 1, \ldots, m \\ & g_i(\mathbf{x}) \leq 1, \ i = 1, \ldots, p \\ & h_i(\mathbf{x}) \leq 1, \ i = 1, \ldots, q \end{aligned} \tag{4.11}$$

where the constraints $f_i(\mathbf{x})$ and $g_i(\mathbf{x})$ are GP compatible, while the constraints $h_i(\mathbf{x})$ are

not and may not even be explicit. Ideally, a general SGP algorithm will mimic the same flexibility of a SQP, and maintain the convex benefits of a GP. We will propose a heuristic algorithm which meets these criteria, but first, let us consider a generalization of iterative methods.

4.4 General Iterative Methods with Black Boxes

Based on the SQP algorithm and previous work in iterative GP solution methods, we can extrapolate a generalized sequential optimization algorithm which utilizes calls to a black box analysis, summarized in the flowchart below:

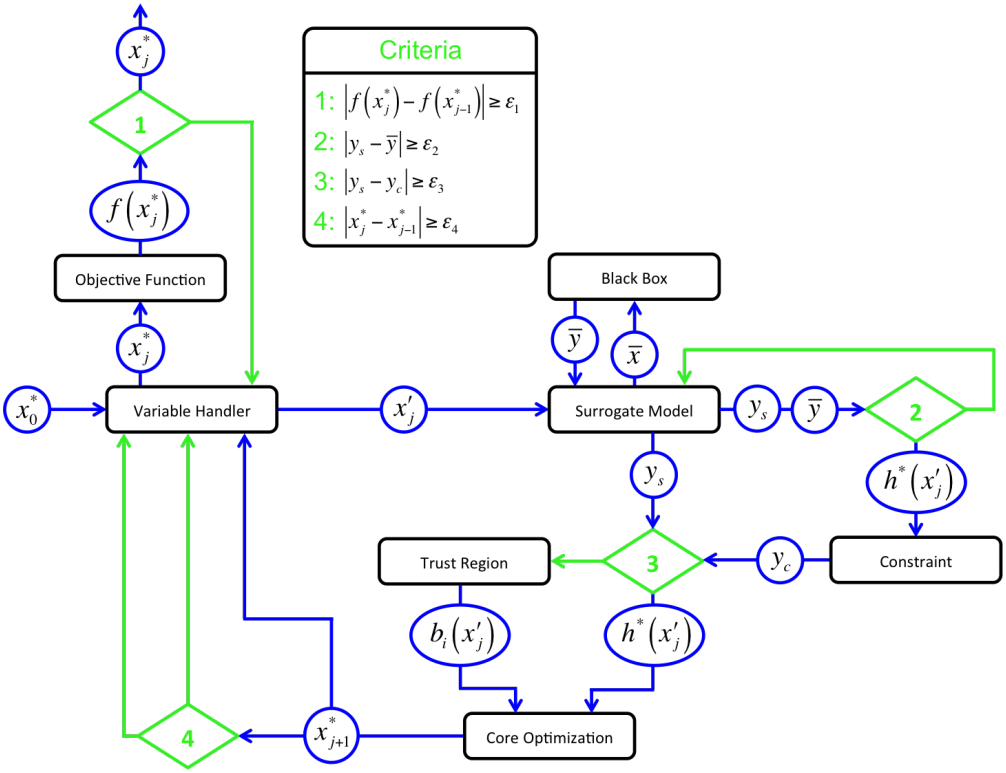

Figure 4-5: Detailed flowchart of iterative optimization methods

A sequential geometric programming algorithm also follows this same flowchart. In the next chapter, we will discuss this flowchart at length and propose a SGP heuristic algorithm.

Chapter 5

Proposal for a Heuristic Sequential Geometric Programming Algorithm

5.1 Algorithm Introduction

Figure 4-5 outlines a generalized sequential algorithm which utilizes a black boxed constraint, but our interest is specifically the practical implementation of a sequential geometric programming algorithm. In this chapter, we will step through the various nodes in Figure 4-5 and discuss how each node functions in the proposed heuristic algorithm.

The proposed SGP algorithm will follow the same high level architecture outlined in Figure 4-5. An initial guess, $\mathbf{x}_0^*$, is passed in and used to create a sampling region for the black box. These samples are then used to create a surrogate model of the black box. The surrogate will then be transformed into a GP compatible constraint, $h^*(\mathbf{x})$, and passed into the GP approximation for that iteration. The GP is solved, a new point is generated and then the process continues until convergence is reached.

5.2 Initialization

Selecting a good initial guess is crucial to the success of sequential algorithms [37], and therefore must be given special consideration. However, with an SGP algorithm, a standard practice is readily available. Using analysis methods such as those proposed by Hoburg [25], a GP compatible constraint can be used in place of the black boxed constraint and the GP solved. In most cases, this will provide a high quality initial guess for the SGP algorithm to begin. While this approach may require a non-trivial effort in some cases, the ability to readily generate an initial guess through the use of a low fidelity GP is a substantial advantage the SGP algorithm has over others.

5.3 Variable Handling

The variable handler cell is a construct of the flow chart and serves as a stand in for some of the logic of the algorithm. At the beginning of each iteration, the entire design vector $\mathbf{x}_j^*$ will be available for processing. The variable handler takes this design vector and serves as a filter for two downstream steps. First, the handler passes the required design variables into the objective function for evaluation. Second, the handler passes the relevant design values into the appropriate surrogate models. In the case of a single black box constraint, the variable handler will only be responsible for processing one set of variables, however, where multiple black boxes are used, multiple sets will be passed downstream. For this work, we will only utilize a single black box constraint.

5.4 Surrogate Modeling

A surrogate model is simply a function which mimics the black box as closely as possible while being less expensive to evaluate. Many options for surrogate models exist, including

simple functions such as posynomials and more complex functions such as Gaussian Process models. The choice of surrogate model and constraint form are inherently coupled, and two extreme options exist for how the two should work together. First, a high fidelity surrogate can be utilized, which captures all of the details of the black box but is not compatible with the underlying optimization. In this case, a procedure must be generated which converts this high fidelity surrogate into a compatible constraint. Using a high fidelity surrogate model ensures the black box is modeled well, but often comes at the price of increased computational expense to call the number of points required to fit the high order surrogate. As a result, this approach should be taken for black box functions that require a high fidelity surrogate to be represented, for example when small perturbation of the inputs result in large changes in the outputs over the region of interest.

Another situation in which high fidelity surrogates should be considered is when the underlying black box itself is thought to be highly incompatible with the core optimization, in this case, when a black box is poorly approximated as GP compatible. In these cases, the convex-concave procedure provides an avenue for solution. For any general black box which can be represented by a Taylor Series, the black box can be equally well represented by a signomial. Then, by the CCP, a signomial program can be relaxed into a GP and solved. This approach will be the subject of future work.

At the other extreme, we can limit ourselves to surrogate models which are compatible with the underlying optimization. A SQP takes this approach to the extreme, using only linear surrogate models for the black box at each iteration. This approach is lightweight computationally, requiring only a few points to be calculated at each iteration, but should only be used with black boxes which are well approximated by GP compatible functions. One additional benefit of this approach is that the surrogate model can directly pass itself into the optimization, eliminating the need to ensure the constraint matches the surrogate, as is required for a high fidelity surrogate model. However, the obvious limitation here is that some black boxes will be poorly approximated by these low fidelity functions and so

convergence may be poor, or the problem may even infeasible.

For this work, we will be utilizing only black boxes which are well approximated by GP compatible functions, and will thus exclusively use surrogate models which are GP compatible.

5.5 Black Box Considerations

Black box analysis codes were covered in some depth in Chapter 2. In the SGP algorithm, the black box receives inputs from the surrogate model and provides outputs back for some number of points contained within a sampling region. A few considerations, first, the black box must be valid over the entire region being considered. For some off the shelf packages, this may require some modification or a wrapper which fills in regions for which the black box is not valid. Alternatively, a black box can also come with a set of constraints to be implemented by the GP.

5.6 Creating GP Compatible Constraints

5.6.1 Soft-Max Affine (SMA) Functions

To create GP compatible constraints from the surrogate models, we require a mathematical form that is of posynomial construction. Hoburg [30] proposes a few functions which are GP compatible to be used for data fitting: max affine (MA), softmax affine (SMA), and implicit softmax affine (ISMA). For the purpose of this work, we will use the SMA function for all black box fitted constraints. An SMA function can be written as:

$$1 \geq \frac{1}{x_1^{\alpha}} \sum_{i=1}^{M} c_i \prod_{j=2}^{N} x_j^{a_{i,j}} \tag{5.1}$$

As discussed in Section 5.4, in our approach for this work we fit an SMA function directly to the black box data. Thus in practice, the surrogate model and SMA GP compatible constraint act as one object. We therefore must develop methodology for linking the black box with the SMA constraint/surrogate model. There are three considerations for this process: the number of terms used by the SMA function to model the black box, the interval over which to sample, and how to select points within that interval.

5.6.2 Number of SMA Terms

An SMA function with M terms and N independent variables requires $M(N+1)+1$ data points to be returned from the black box function, and so clearly selecting the correct number of SMA fitting terms has the single largest impact on the number of black box calls made during the run of the algorithm. Given the critical nature of this consideration, we leave it exposed as a setting that can be selected by the designer. In practice, we observe that a good choice is to use a number of terms equal to the number of inputs to the black box. This provides the fitting algorithm with enough flexibility to fit the data, while minimizing the number of calls that must be made.

5.6.3 Interval of Sampling

Two extremes exist for selecting a sample interval: a large region which captures the global trends of the black box, or a local region which captures the details near the current design point. Between these two extremes is a continuous spectrum of options, illustrated by the figure below:

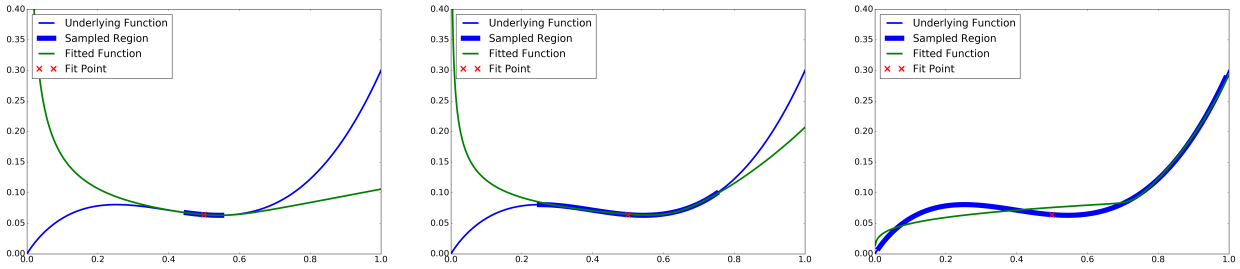

(a) Local Interval (b) Intermediate Interval (c) Full Interval

Figure 5-1: Impact of sampling interval on fit

Note that there is a trade-off between local error and global error. As the sampling region approaches the full interval, global error decreases at the cost of local error. Selection on this spectrum is non obvious, even for functions that are well approximated by a SMA function as we have assumed. In the early iterations, we want to capture the global trend of the black box, but when approaching convergence, local error should be driven down. Thus, we propose a mechanism for changing the interval as the algorithm iterates, favoring a global sampling region early and then moving to a local interval.

Two user defined parameters control the interval. First, an initial interval is explicitly defined by the user, as a percentage multiplier and divisor on the initial guess. Second, a parameter is defined that tunes the rate at which the interval decreases in size, slowly progressing to a local sampling region. This value is the percent of the previous interval to be taken in the next iteration.

When approaching final convergence, an SMA fit on a highly local region will still produce local model error at the design point, despite high confidence that the design point is correct. We therefore desire a new fitting function that ensures minimal error at the point under consideration, roughly analogous to using a linear fit at the termination of an iterative algorithm. Boyd [27] provides a general monomial approximation scheme for any function:

$$f(\mathbf{x}) \approx f(\mathbf{x}^*) \prod_{i=1}^{n} \left(\frac{x_i}{x_i^*} \right)^{a_i}$$
$$a_i = \frac{x_i^*}{f(\mathbf{x}^*)} \frac{\partial f}{\partial x_i^*} \tag{5.2}$$

which ensures minimal error at $\mathbf{x}^*$ and creates a good local approximation. When the sampling interval decreases in size to a certain user specified value, the algorithm flips into a monomial fitting mode to remove as much local error as possible.

5.6.4 Selecting Points in the Interval

A final consideration is how to select points within the interval once it has been defined. Our algorithm simply casts an evenly spaced grid over the N dimensional interval, and does this with every iteration, saving none of the data from previous iterations. This is an area that could be significantly improved by future work.

5.7 Implementing Trust Regions

In cases where the surrogate model diverges from the constraint beyond the local region, trust regions should be used to constrain the optimizer. A trust region is easy to implement in a GP as the percent change of the design variable with respect to the previous value. In this case, trust regions were implemented whenever monomial constraints were used, as monomials can vary widely from the surrogate model beyond the local region of the design variable.

5.8 Convergence Criteria

Figure 4-5 outlines four criteria which must be true at convergence:

1. The change in objective between iterations must be small

2. The surrogate model must accurately represent the black box

3. The constraint must accurately represent the surrogate

4. The change in the design variable values must be small

The first criteria compares the value of the objective function at the current design point with the value of the objective function at the previous design point. A common metric for iterative algorithms, when the difference between these two values is large, it indicates that the algorithm has not yet converged to the optimal design point and so the algorithm continues iterating. As the algorithm iterates, this difference will continue to get smaller until the relative tolerance is satisfied and the algorithm then returns the converged design. See Figure 4-2 for a graphical example.

The second criteria compares the outputs variables of the black box with the output variables of the surrogate model for the same set of inputs. In most cases, the surrogate will not match the black box for all points even under the best of circumstances, and so the meaning of this metric will vary on a case by case basis. However, regardless of application the surrogate will have to match the black box at the final design point in order to ensure convergence.

The third criteria compares the dependent variables of the constraint with the dependent variables of the surrogate model. Since this approach utilizes the surrogate directly as a constraint in the GP solve, this error is by definition zero.

The fourth criteria compares the design variables between the current iteration and the last iteration. Similar to the first criteria, when the design values are changing substantially it implies that the optimal design may not have been reached. Thus, we can implement the additional criteria that the relative change in design variables should be small and handle this criteria in the same way as the relative tolerance criteria. In practice, we do not implement any such constraints, but the discussion is included here for comprehensiveness.

Chapter 6

Implementation of the Sequential Geometric Programming Algorithm on a Solar Powered Aircraft

6.1 Solar Aircraft Test Problem

Recent work by Burton and Hoburg [40] produced a GP compatible model for conceptual design of solar powered HALE aircraft. This model optimizes 166 design variables, and captures trades in a non-intuitive design space. The full results of Burton's GP are included in Appendix A. We selected this problem to test the SGP algorithm on, specifically the profile drag model.

Burton's original model contains a GP compatible equation for profile drag:

$$C_{D_p}^{3.72} \geq 0.0247 C_L^{2.49} Re^{-1.11} + 2.03 \times 10^{-7} C_L^{12.7} Re^{-0.338} + 6.35 \times 10^{10} C_L^{-0.243} Re^{-3.43} + 6.49 \times 10^{-6} C_L^{-1.9} Re^{-0.681} \tag{6.1}$$

The first step was to modify this constraint to include τ, which is also a critical parameter for airfoil selection. Hoburg [25] previously provided just such a constraint based on fitting a family of NACA 4-series airfoils:

$$\begin{aligned} 1 \geq\ & 2.56 C_L^{5.88} \tau^{-3.32} Re^{-1.54} C_{D_p}^{-2.62} + 3.8 \times 10^{-9} C_L^{-0.92} \tau^{6.23} Re^{-1.38} C_{D_p}^{-9.57} \\ & + 2.2 \times 10^{-3} C_L^{-0.01} \tau^{0.033} Re^{0.14} C_{D_p}^{-0.73} + 1.19 \\ & \times 10^{4} C_L^{9.78} \tau^{1.76} Re^{-1} C_{D_p}^{-0.91} + 6.14 \times 10^{-6} C_L^{6.53} \tau^{-0.52} Re^{-0.99} C_{D_p}^{-5.19} \end{aligned} \tag{6.2}$$

While a NACA 4-series airfoil would be a poor selection of airfoil for a HALE solar powered aircraft, this constraint provides us with a tested example which relates the variables of interest.

This case is the baseline for our remaining work, an entirely GP model which captures the tradeoffs we are interested in. The full results of this baseline case are included in Appendix A.

While the ultimate goal of this work is to implement a high fidelity black box such as those mentioned in Chapter 2, our immediate goal is to evaluate the performance of the SGP algorithm. Thus, Equation 6.2 was placed into a black box, returning a profile drag for a given set of inputs for C_L, Re, and τ. This enables a common comparison between the algorithm and a known GP solution.

In summary, we have two cases to consider:

- Case 1: Equation 6.2 implemented directly as a GP constraint, solved as a GP
- Case 2: Equation 6.2 implemented as a black box, solved as an SGP

6.2 User Defined Inputs

Many parameters are available to the user and are summarized here for clarity.

6.2.1 Initial Guess Values

parameters.clguess, parameters.reguess, parameters.tauguess
These parameters provide an initial guess for the SGP algorithm to begin iterating. Note that initial guesses are not required for all design variables, only those used in the black box constraint.

6.2.2 SMA Model Parameters

parameters.fit_ order
This value sets the number of terms used in the SMA fitting function. In the current algorithm, this number remains fixed throughout all iterations, but future work may explore allowing this number to be actively controlled by the algorithm.

6.2.3 Initial Sampling Interval Parameters

parameters.cl_ band, parameters.re_ band, parameters.tau_ band
These values set the initial sampling interval, or "band" for the SGP algorithm. The user specifies these values as a fraction of the initial guess. For example, a value:

```
parameters.cl_band = 0.5
```

corresponds to an initial sampling from $0.5C_L^*$ to $1.5C_L^*$.

6.2.4 Sampling Interval Tightening Parameters

parameters.cltighten, parameters.retighten, parameters.tautighten

These parameters set the rate at which the sampling interval tightens as percent of the previous interval. For example, a value:

```
parameters.cltighten = 0.9
```

would result in 90% of the previous interval being preserved at the next iteration. Therefore, the first iteration would be 90% of the initial interval, the second 81% and so on.

parameters.band_min

Value sets the limit at which the algorithm switches into monomial mode. A nominal value of 10% of the initial interval has worked well for this work, but future work may study more rigorous selection of this value.

6.2.5 Monomial Mode Parameters

parameters.monomial_fd_band

This value sets the perturbation for the finite differencing scheme as a fraction of the initial guess and is generally set to a small value.

parameters.trust_region

This value sets up the trust region implemented when the algorithm flips to monomial mode. The following constraints are implemented:

$$
\begin{aligned}
\frac{C_L}{C_L^*} &\leq 1 + parameters.trust\_region \\
\frac{C_L}{C_L^*} &\geq 1 - parameters.trust\_region \\
\frac{Re}{Re^*} &\leq 1 + parameters.trust\_region \\
\frac{Re}{Re^*} &\geq 1 - parameters.trust\_region \\
\frac{\tau}{\tau^*} &\leq 1 + parameters.trust\_region \\
\frac{\tau}{\tau^*} &\geq 1 - parameters.trust\_region
\end{aligned}
\tag{6.3}
$$

parameters.modelTol

This value sets the tolerance for Convergence Criteria 2 as outlined in Chapters 4 and 5.

Chapter 7

Results of the Sequential Geometric Programming Algorithm

7.1 Success Metrics

There are two key success metrics for the algorithm. First, the algorithm should return a result similar to the directly implemented GP model, ie, the algorithm should achieve the optimal design point within a small error. Second, the number of black box calls should be minimized, as calls to the black box are assumed in general to be computationally expensive.

Additionally, we expect that a good algorithm would be robust to various values for the initial guess and the tuning parameters outlined in Chapter 6.2. Thus, we will sweep over these values and recover performance in both metrics to validate a robust algorithm.

7.2 Algorithm Performance

Taking the initial guesses for C_L, Re and τ to be 90% of their known optimal values and using reasonable tuning parameters (0.4 for band values and 0.65 for tightening values), we see the following results:

Table 7.1: Comparing Solar Aircraft Results

	Case 1	Case 2	Error
Black Box Calls	-	120	-
W_{total} (lbf)	59.5589	59.5598	0.00%
C_{D_p}	0.0137	0.0138	0.28%
C_D	0.0198	0.0200	0.79%
C_L	0.8860	0.8889	0.33%
τ	0.2714	0.2700	-0.51%
Re	95233.3337	95620.8497	0.41%
V (m/s)	28.8922	28.8403	-0.18%
P_{max} (W)	265.2127	265.5984	0.15%
S (ft^2)	55.3864	55.4670	0.15%
A	45.5262	44.9616	-1.24%
MAC (ft)	1.1030	1.1107	0.70%
b (ft)	50.2149	49.9388	-0.55%
W_{wing} (lbf)	15.7429	15.7346	-0.05%
$W_{battery}$ (lbf)	24.8680	24.9041	0.15%

The full results of the SGP algorithm are included in Appendix A. Note that the overall objective exhibits less than a one percent error, with the largest design variable error being less than two percent. The algorithm also required only 120 calls to the black box which would be quite reasonable for a black box code such as XFOIL. The convergence of the algorithm is shown in the plot below:

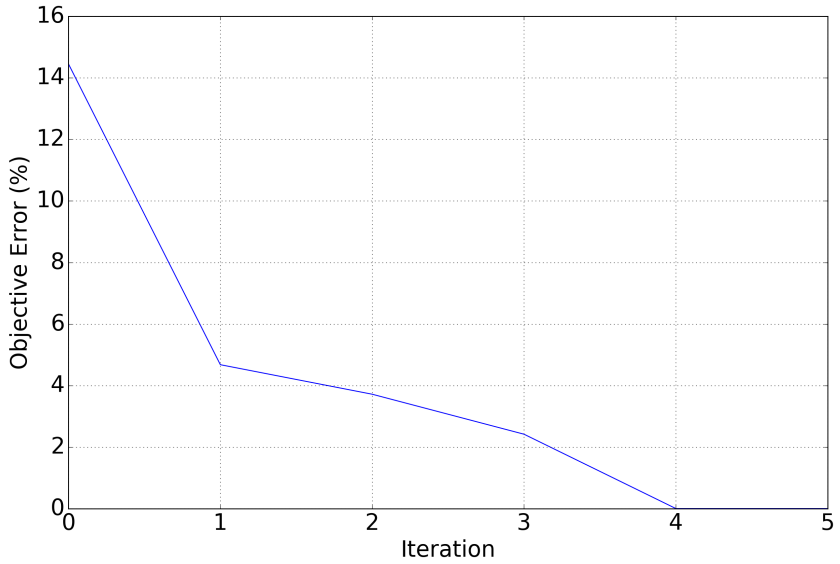

Figure 7-1: Convergence of the SGP Algorithm

Considering algorithm robustness, we swept over three of the user defined inputs mentioned in Chapter 6.2: initial guess, initial interval, and interval tightening. The two parameters not under consideration were fixed during the sweep at well behaving nominal values. Ideally, we would observe that as these user inputs vary, the overall error in the objective function between Case 1 and Case 2 will remain small, and the number of black box calls will also remain low.

Sweeping the initial guess from 50% of the known optimum to 150% of the known optimum, we see the following results:

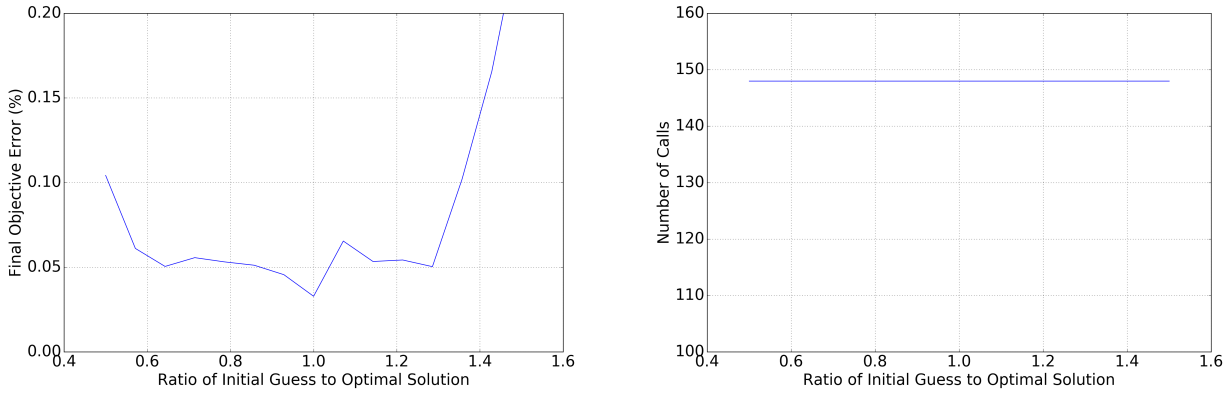

(a) Error in Objective

(b) Number of Calls

Figure 7-2: Impact of changing the initial guess of Case 2

As might be expected, we see a minimum error near an initial guess of exactly the known optimum, and an increasing error as we move away from that best guess. Note that for most of these trials, the absolute error between the objective functions of Case 1 and Case 2 are less than 0.1%. Interesting however is that the number of black box calls stays the same as we sweep over the initial guesses. This is primarily due to the fact that the number of SMA iterations remains the same, as the intervals change in the same way in every case and only one monomial fit is required to reach model tolerance. If the required model tolerance were tightened, we might expect different behavior.

Considering the initial interval, we observe the following results:

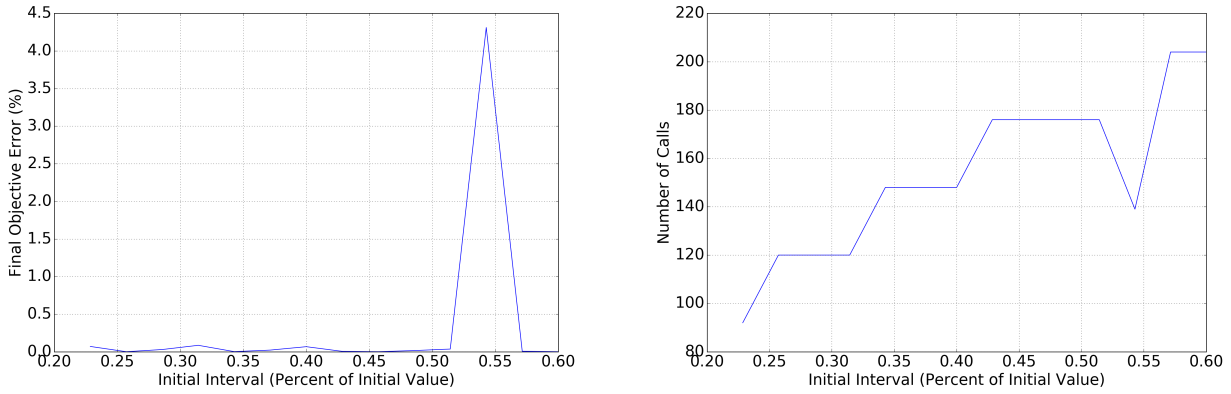

(a) Error in Objective

(b) Number of Calls

Figure 7-3: Impact of changing the initial interval of Case 2

The x-axis here is the initial band value discussed in Chapter 6.2. These results are quite interesting. First, we observe a spike in error at around 0.55. Coupled with the comparatively low number of black box calls at this point, this error is likely due one an early GPkit termination, however less than 5% error is still observed. Additionally, the stair-step in the number of calls is due to the logic which changes to monomial mode. Each step represents an additional SMA call before the monomial mode is activated, since as the initial interval gets bigger, it takes more steps to reach the fixed value where the mode changes.

Finally, we consider the rate at which we tighten the interval:

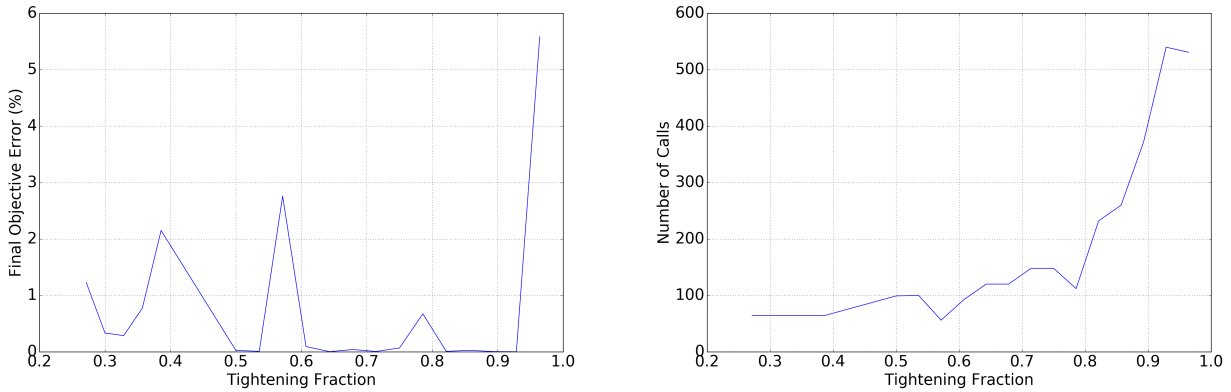

(a) Error in Objective

(b) Number of Calls

Figure 7-4: Impact of changing the tightening rate of the interval of Case 2

The x-axis here is the tightening value discussed in Chapter 6.2. Sweeping this parameter results in the most error in the objective, with no discernible trend. However, as expected, the number of calls increases as the ratio of preserved interval increases, resulting in more SMA iterations. Based on these results, a value between 0.6 and 0.8 seems most appropriate.

Chapter 8

Conclusions and Future Work

8.1 Summary

Geometric programming (GP) has proven a valuable tool in the conceptual aircraft design space, however the GP formulation prevents the use of black box analysis tools that are prolific in the MDAO community. This work extends the GP formulation, enabling a black box drag polar to be utilized during conceptual design. A sequential geometric programming algorithm was developed based on the previous work in sequential convex programming, and applied successfully to a solar powered HALE aircraft with less than 1% error in the final objective. This work lays the groundwork for a new opportunity in GP, bringing it closer to more classical MDAO formulations and expanding its practicality in real design problems.

8.2 Future Work

8.2.1 Utilizing Signomial Surrogate Models

The next step for this work is to implement a signomial surrogate modeling approach. This would first require a general signomial fitting algorithm which does not yet exist. Once this algorithm has been written, methods for relaxing signomial constraints into posynomials (via similar methods to the CCP) must be developed and the algorithm tested on a new test problem.

A more long term vision for surrogate models would be to implement something like a Gaussian Process which could incorporate a measure of uncertainty quantification in addition to the deterministic values provided by a SMA or signomial fit. This type of method could significantly reduce the number of black box calls required to converge to an optimum.

8.2.2 Implementing New Black Boxes

Once the signomial surrogate has been implemented, non-convex black boxes can be implemented. We would start with XFOIL [41], a low fidelity aero code which has been utilized in some previous work, and then progress up the fidelity tree. Other disciplines such as weights and propulsion must also be investigated and may prove more difficult than aerodynamic databases which tend to be nearly log-convex.

One more interesting future avenue for expanding black boxes is to utilize a black box to perform multi-level optimization. In many cases, a designer must make decisions that are simply too detailed to be captured in the GP or SGP, for example, the detailed airfoil shape on a wing or the number of turbine blades in a compressor. If desired, these detailed decisions can be left as free variables in the black box, resulting in an additional level of

optimization. If this freedom is utilized correctly, the output of a black box code will be a Pareto Front rather than a pure analysis output.

8.2.3 Developing a General SGP Algorithm

Perhaps the ultimate vision of this work is to develop a general SGP algorithm. Such an algorithm would exhibit the same flexibility of a SQP algorithm, while retaining many of the advantages of sequential convex programs such as DOC. A great deal of work and study must be done to reach this vision, but given the role geometric programming is beginning to play in aircraft design, an SGP algorithm could have a great impact on the future of aircraft design.

Bibliography

[1] Blanchard, B. S. and Fabrycky, W. J., *Systems Engineering and Analysis*, Vol. 4, Prentice Hall Englewood Cliffs, NJ, 1990.

[2] http://www.aurora.aero/d8/.

[3] "Systems Architecture Concept Generation," http://ocw.mit.edu/courses/aeronautics-and-astronautics/16-842-fundamentals-of-systems-engineering-fall-2009/lecture-notes/MIT16_842F09_lec04.pdf, 2009.

[4] Patt, D., "Time: Development/Fielding Time, Composability, and Architectures," 2012.

[5] Torenbeek, E., *Synthesis of Subsonic Airplane design*, Kluwer Academic Publishers, Dordrecht, The Netherlands, 2nd ed., 1982.

[6] "Systems Architecture: An Overview and Agenda," http://web.mit.edu/deweck/www/PDF_archive/4%20Other%20Major%20Pubs/4_2_AFOSR_MIT-Crawley_deWeck.pdf, 2002.

[7] Lazzara, D. S., *Modeling and Sensitivity Analysis of Aircraft Geometry for Multidisciplinary Optimization Problems*, Ph.D. thesis, Massachusetts Institute of Technology, Cambridge, Massachusetts, May 2012.

[8] Haimes, R. and Dannenhoffer III, J. F., "The Engineering Sketch Pad: A Solid-Modeling, Feature-Based, Web-Enabled System for Building Parametric Geometry," *21st AIAA Computational Fluid Dynamics Conference*, San Diego, CA, June 2013.

[9] Anderson, J. D., *Aircraft Performance and Design*, WCB McGraw-Hill, Boston, Massachusetts, 1999.

[10] https://www.nasa.gov/content/hybrid-wing-body-goes-hybrid.

[11] Raymer, D. P., *Aircraft Design: A Conceptual Approach*, American Institute of Aeronautics and Astronautics, Reston, Virginia, 4th ed., 2006.

[12] Roskam, J., "Airplane Design: Part I-VIII," *DAR Corporation, Lawrence, KS*, 2006.

[13] Shevell, R. S., *Fundamentals of Flight*, Pretence Hall, Upper Saddle River, NJ, 2nd ed., 1989.

[14] Schaufele, R. D., *The Elements of Aircraft Preliminary Design*, Aries Publications, Santa Ana, California, 2000.

[15] Drela, M., "Development of the D8 Transport Configuration," *29th AIAA Applied Aerodynamics Conference*, Honolulu, Hawaii, June 2011.

[16] Liebeck, R. H., "Design of the Blended Wing Body Subsonic Transport," *Journal of Aircraft*, Vol. 41, No. 1, January-February 2004, pp. 10–25.

[17] Kroo, I. and Takai, M., "A Quasi-Procedural, Knowledge-Based System for Aircraft Design," *AIAA Paper AIAA-88-6502*, 1988.

[18] Wakayama, S., "Multidisciplinary Design Optimization of the Blended-Wing-Body," *AIAA Paper AIAA-98-4938*, 1998.

[19] Lukaczyk, T., Wendorff, A. D., Botero, E., MacDonald, T., Momose, T., Variyar, A., Vegh, J. M., Colonno, M., Economon, T. D., Alonso, J. J., Orra, T. H., and Ilario da Silva, C., "SUAVE: An Open-Source Environment for Multi-Fidelity Conceptual Vehicle Design," *16th AIAA/ISSMO Multidisciplinary Analysis and Optimization Conference*, Dallas, Texas, June 2015.

[20] von Kaenel, R., Rizzi, A., Oppelstrup, J., Goetzendorf-Grabowski, T., Ghoreyshi, M., Cavagna, L., and Berard, A., "CEASIOM: Simulating Stability & Control with CFD/CSM in Aircraft Conceptual Design," *26th International Congress of the Aeronautical Sciences, ICAS*, 2008.

[21] Drela, M., "TASOPT 2.00," Tech. rep., Massachusetts Institute of Technology, March 2010.

[22] Martins, J. R. and Lambe, A. B., "Multidisciplinary Design Optimization: A Survey of Architectures," *AIAA Journal*, Vol. 51, No. 9, 2013, pp. 2049–2075.

[23] Price, M., Raghunathan, S., and Curran, R., "An Integrated Systems Engineering Approach to Aircraft Design," *Progress in Aerospace Sciences*, Vol. 42, No. 4, 2006, pp. 331–376.

[24] Boyd, S. and Vandenberghe, L., *Convex Optimization*, Cambridge University Press, Cambridge, UK, 7th ed., 2009.

[25] Hoburg, W. and Abbeel, P., "Geometric Programming for Aircraft Design Optimization," *AIAA Journal*, Vol. 52, No. 11, 2014, pp. 2414–2426.

[26] Floudas, C. A., *Nonlinear and Mixed-Integer Optimization: Fundamentals and Applications*, Oxford University Press, New York, 1995.

[27] Boyd, S., Kim, S.-J., Vandenberghe, L., and Hassibi, A., "A Tutorial on Geometric Programming," *Optimization and Engineering*, Vol. 8, No. 1, 2007, pp. 67–127.

[28] Cramer, E. J., Dennis, Jr, J., Frank, P. D., Lewis, R. M., and Shubin, G. R., "Problem Formulation for Multidisciplinary Optimization," *SIAM Journal on Optimization*, Vol. 4, No. 4, 1994, pp. 754–776.

[29] Burnell, E. and Hoburg, W., "GPkit software for geometric programming," https://github.com/hoburg/gpkit, 2015, Version 0.4.1.

[30] Hoburg, W., Kirschen, P., and Abbeel, P., "Data fitting with geometric-programming-compatible softmax functions," *Optimization and Engineering*, 2016, pp. 1–22.

[31] MIT Convex Optimization Group, "GPfit," https://github.com/convexopt/gpfit, 2015, Version 0.1.

[32] Hileman, J. I., Spakovszky, Z. S., Drela, M., and Sargeant, M. A., "Airframe Design for "Silent Aircraft"," *45th AIAA Aerospace Sciences Meeting and Exhibit*, Reno, Nevada, January 2007.

[33] Nocedal, J. and Wright, S., *Numerical Optimization*, Springer Science & Business Media, 2006.

[34] Boggs, P. T. and Tolle, J. W., "Sequential Quadratic Programming," *Acta Numerica*, Vol. 4, 1996, pp. 1–51.

[35] Maranas, C. D. and Floudas, C. A., "Global Optimization in Generalized Geometric Programming," *Computers & Chemical Engineering*, Vol. 21, No. 4, 1997, pp. 351–369.

[36] Kirschen, P. G., Burnell, E. E., and Hoburg, W. W., "Signomial Programming Models for Aircraft Design," *54th AIAA Aerospace Sciences Meeting*, 2016.

[37] Boyd, S., "Sequential Convex Programming," 2015, lecture notes of EE364b, Stanford University, Spring Quarter.

[38] Lipp, T. and Boyd, S., "Variations and extensions of the convex–concave procedure," *Optimization and Engineering*, 2014, pp. 1–25.

[39] Charafeddine, M. and Paulraj, A., "Sequential Geometric Programming for 2× 2 Interference Channel Power Control." *CISS*, 2007, pp. 185–189.

[40] Burton, M., "Gas/Solar Trade," https://github.com/hoburg/gas_solar_trade, April 2017.

[41] Drela, M., "XFOIL: An Analysis and Design System for Low Reynolds Number Airfoils," *Low Reynolds Number Aerodynamics*, Springer, 1989, pp. 1–12.

Appendix A

Full Report of Design Results

A.1 Original Formulation From Burton

Cost

---

122 [lbf]

Free Variables

Mission, Aircraft |			
W_{cent} :	31.27	[lbf]	center weight
W_{total} :	122	[lbf]	aircraft weight
W_{wing} :	90.71	[lbf]	wing weight
Mission, Aircraft, Battery |			
E :	2.949e+07	[J]	total battery energy
W :	51.62	[lbf]	battery weight
\mathcal{V} :	0.06126	[m**3]	battery volume
Mission, Aircraft, Empennage |			
W :	20.98	[lbf]	empennage weight
Mission, Aircraft, Empennage, HorizontalTail |			
AR_h :	14.34		horizontal tail aspect ratio
C_{L_{max}} :	1.5		maximum CL of horizontal tail
S :	9.112	[ft**2]	horizontal tail area
W :	1.663	[lbf]	horizontal tail weight
b :	11.43	[ft]	horizontal tail span
c_{r_h} :	0.8858	[ft]	horizontal tail root chord
c_{t_h} :	0.7086	[ft]	horizontal tail tip chord
l_h :	11.11	[ft]	horizontal tail moment arm
Mission, Aircraft, Empennage, TailBoom |			
I_0 :	1.676e-06	[m**4]	tail boom moment of inertia
J :	1.676e-06	[m**4]	tail boom polar moment of inertia
S :	10.48	[ft**2]	tail boom surface area
W :	11.49	[lbf]	tail boom weight
d_0 :	3.602	[in]	tail boom diameter
l :	11.11	[ft]	tail boom length
t_0 :	5.571	[mm]	tail boom thickness
Mission, Aircraft, Empennage, VerticalTail |			
AR_v :	4.427		vertical tail aspect ratio
S :	24.3	[ft**2]	total vertical tail surface area
W :	7.831	[lbf]	one vertical tail weight
b :	10.37	[ft]	one vertical tail span
c_{r_v} :	2.756	[ft]	vertical tail root chord

```
                                            c_{t_v} : 1.929                                        [ft]      vertical tail tip chord
                                                l_v : 11.11                                        [ft]      horizontal tail moment arm

                           Mission, Aircraft, Engine |
                                            P_{max} : 550.5                                        [W]       max power
                                                  W : 0.2932                                       [lbf]     engine weight
                                                  m : 0.1329                                       [kg]      engine mass

                       Mission, Aircraft, SolarCells |
                                                  S : 115                                          [ft**2]   solar cell area
                                                  W : 6.36                                         [lbf]     solar cell weight

Mission, AircraftLoading, EmpennageLoading, HorizontalBoomBending |
                                                  F : 1556                                         [N]       horizontal tail force
                                             \theta : 0.07997                                                tail boom deflection angle

  Mission, AircraftLoading, EmpennageLoading, VerticalBoomBending |
                                                  F : 2433                                         [N]       vertical tail force
                                             \theta : 0.1                                                    tail boom deflection angle

  Mission, AircraftLoading, EmpennageLoading, VerticalBoomTorsion |
                                                  T : 7692                                         [N*m]     vertical tail moment

                Mission, AircraftLoading, WingLoading, ChordSparL |
                                          \vec{M_r} : [ 1.89e+03  918       377       92.6     ]   [N*m]     wing section root moment

          Mission, AircraftLoading, WingLoading, ChordSparL, Beam |
                                                 dx : 0.25                                                   normalized length of element
                                    \vec{\bar{EI}} : [ 1.68      0.829     0.299     0.0469   ]             normalized YM and moment of inertia
                                     \vec{\bar{M}} : [ 0.607     0.295     0.121     0.0297   ... ]         normalized moment
                                     \vec{\bar{S}} : [ 1.37      0.794     0.456     0.2      ... ]         normalized shear
                                 \vec{\bar{\delta}} : [ 8.69e-05  0.0151    0.0517    0.109    ... ]         normalized displacement
                                      \vec{\theta} : [ 0.000458  0.0752    0.151     0.237    ... ]         deflection slope

                    Mission, AircraftLoading, WingLoading, GustL |
                                          \vec{M_r} : [ 2.56e+03  1.58e+03  761       202      ]   [N*m]     wing section root moment
                                 \vec{\alpha_{gust}} : [ 8.85e-11  0.0309    0.113     0.231    ... ]         gust angle of attack
                                     \vec{\bar{q}} : [ 1.33      1.9       3.29      4.74     ... ]         normalized loading

               Mission, AircraftLoading, WingLoading, GustL, Beam |
                                                 dx : 0.25                                                   normalized length of element
                                    \vec{\bar{EI}} : [ 4.61      2.45      0.989     0.2      ]             normalized YM and moment of inertia
                                     \vec{\bar{M}} : [ 2.05      1.27      0.611     0.162    ... ]         normalized moment
                                     \vec{\bar{S}} : [ 3.35      2.95      2.3       1.3      ... ]         normalized shear
```

```
                                \vec{\bar{\delta}} : [ 2.07e-05  0.013     0.0498    0.111    ... ]             normalized displacement
                                     \vec{\theta} : [ 0.000173  0.092     0.19      0.291    ... ]             deflection slope

                    Mission, FlightSegment, AircraftPerf |
                                              CDA : 0.004203                                                   non-wing drag coefficient
                                              C_D : 0.03848                                                    aircraft drag coefficient
                                         P_{oper} : 550.5                                    [W]           operating power
                                        P_{shaft} : 0.7383                                   [hp]          shaft power

            Mission, FlightSegment, AircraftPerf, TailAero |
                                              C_d : 0.01821                                                    horizontal tail drag coefficient
                                              C_d : 0.009711                                                   vertical tail drag coefficient
                                               Re : 5.631e+04                                                  horizontal tail reynolds number
                                               Re : 1.655e+05                                                  vertical tail reynolds number

        Mission, FlightSegment, AircraftPerf, TailBoomAero |
                                              C_f : 0.007754                                                   fuselage skin friction coefficient
                                               Re : 7.851e+05                                                  fuselage reynolds number

            Mission, FlightSegment, AircraftPerf, WingAero |
                                              C_L : 1.21                                                       lift coefficient
                                              C_d : 0.03428                                                    wing drag coefficient
                                               Re : 1.383e+05                                                  Reynold's number
                                            c_{dp} : 0.01702                                                   wing profile drag coeff

                    Mission, FlightSegment, FlightState |
                                          (E/S)_C : 193.2                                [W*hr/m**2]   energy for batteries during sunrise/set
                                       (E/S)_{day} : 2159                                [W*hr/m**2]   solar cells energy during daytime
                                       (P/S)_{min} : 234.3                               [W/m**2]      minimum necessary solar power
                                                 V : 25.52                               [m/s]         true airspeed
                                         V_{wind} : 25.52                                [m/s]         wind velocity
                                             \rho : 0.129                                [kg/m**3]     air density

                Mission, FlightSegment, SteadyLevelFlight |
                                                 T : 17.26                               [N]           thrust

                                         Wing |
                                                AR : 30                                                    aspect ratio
                                                 S : 115                                 [ft**2]       surface area
                                                 W : 32.73                               [lbf]         weight
                                              \tau : 0.115                                             airfoil thickness ratio
                                                 b : 58.73                               [ft]          wing span
                                            c_{MAC} : 1.958                              [ft]          mean aerodynamic chord
                                           c_{root} : 2.61                               [ft]          root chord
```

```
                                \vec{c_{ave}} : [ 2.45      2.12      1.79      1.47     ]  [ft]        mid section chord

                                Wing, CapSpar |
                                            W : 3.832                                        [lbf]       spar weight
                                        \vec{I} : [ 3.81e-07  2.04e-07  8.33e-08  1.81e-08 ]  [m**4]      spar x moment of inertia
                                      \vec{S_y} : [ 4.49e-06  2.77e-06  1.34e-06  3.54e-07 ]  [m**3]      section modulus
                                       \vec{dm} : [ 0.388     0.275     0.156     0.0498   ]  [kg]        segment spar mass
                                    \vec{h_{in}} : [ 3.3       2.86      2.43      2.01     ]  [in]        inner spar height
                                        \vec{t} : [ 0.0381    0.0312    0.0209    0.00816  ]  [in]        spar cap thickness
                                        \vec{w} : [ 4.4       3.82      3.23      2.64     ]  [in]        spar width

                               Wing, WingSkin |
                                            W : 23.45                                        [lbf]       wing skin weight
                                            t : 0.012                                        [in]        wing skin thickness

Constants
---------

                             Mission, Aircraft |
                                    W_{pay} : 10                                             [lbf]       payload

                        Mission, Aircraft, Battery |
                          (E/\mathcal{V}) : 800                                              [W*hr/l]    volume battery energy density
                            \eta_{charge} : 0.98                                                         Battery charging efficiency
                         \eta_{discharge} : 0.98                                                         Battery discharging efficiency
                                       g : 9.81                                              [m/s**2]    gravitational constant
                                  h_{batt} : 350                                             [W*hr/kg]   battery energy density

                       Mission, Aircraft, Empennage |
                                   m_{fac} : 1                                                           Tail weight margin factor

          Mission, Aircraft, Empennage, HorizontalTail |
                                     V_h : 0.45                                                          horizontal tail volume coefficient
                          \bar{A}_{NACA0008} : 0.0548                                                    cross sectional area of NACA 0008
                                  \lambda : 0.8                                                          horizontal tail taper ratio
                      \lambda_h/(\lambda_h+1) : 0.4444                                                   horizontal tail taper ratio factor
                                \rho_{foam} : 1.5                                                [lbf/ft**3] Density of formular 250
                                \rho_{skin} : 0.049                                              [g/cm**2]   horizontal tail skin density
                                      \tau : 0.08                                                          horizontal tail thickness ratio
                                         g : 9.81                                              [m/s**2]    Gravitational acceleration
                                       m_h : 5.514                                                         horizontal tail span effectiveness
                                   m_{fac} : 1.1                                                         horizontal tail margin factor

                Mission, Aircraft, Empennage, TailBoom |
                                  (1-k/2) : 0.6                                                          (1-k/2)
```

```
                                                E : 1.5e+11      [N/m**2]    young's modulus carbon fiber
                                        \rho_{CFRP} : 1.6        [g/cm**3]   density of CFRP
                                                g : 9.81         [m/s**2]    Gravitational acceleration
                                                k : 0.8                      tail boom inertia value
                                            m_{fac} : 1                      tail boom margin factor
                                            t_{min} : 0.25       [mm]        minimum tail boom thickness

                          Mission, Aircraft, Empennage, VerticalTail |
                                        C_{L_{max}} : 1.1                    maximum CL of vertical tail
                                                V_v : 0.04                   vertical tail volume coefficient
                                \bar{A}_{NACA0008} : 0.0548                  cross sectional area of NACA 0008
                                           \lambda : 0.7                     vertical tail taper ratio
                                \lambda_v/(\lambda_v+1) : 0.4118             vertical tail taper ratio factor
                                        \rho_{foam} : 1.5        [lbf/ft**3] Density of formular 250
                                        \rho_{skin} : 0.049      [g/cm**2]   vertical tail skin density
                                              \tau : 0.08                    vertical tail thickness ratio
                                                g : 9.81         [m/s**2]    Gravitational acceleration
                                            m_{fac} : 1.1                    vertical tail margin factor

                                    Mission, Aircraft, Engine |
                                         B_{PM} : 4141           [W/kg]      power mass ratio
                                                g : 9.81         [m/s**2]    gravitational constant

                                  Mission, Aircraft, SolarCells |
                                              \eta : 0.22                    Solar cell efficiency
                                      \rho_{solar} : 0.27        [kg/m**2]   solar cell area density
                                                g : 9.81         [m/s**2]    gravitational constant

Mission, AircraftLoading, EmpennageLoading, HorizontalBoomBending |
                                      \theta_{max} : 0.1                     max tail boom deflection angle

       Mission, AircraftLoading, EmpennageLoading, TailBoomState |
                                             V_{NE} : 40         [m/s]       never exceed vehicle speed
                                         \rho_{sl} : 1.225       [kg/m**3]   air density at sea level

  Mission, AircraftLoading, EmpennageLoading, VerticalBoomBending |
                                      \theta_{max} : 0.1                     max tail boom deflection angle

  Mission, AircraftLoading, EmpennageLoading, VerticalBoomTorsion |
                                      \tau_{CFRP} : 210            [MPa]     torsional stress limit

              Mission, AircraftLoading, WingLoading, ChordSparL |
                                          N_{max} : 5                        max loading
                                           \kappa : 0.2                      max tip deflection ratio
```

```
                                \sigma_{CFRP} : 4.7e+08                                  [Pa]         CFRP max stress
                                \vec{\bar{q}} : [ 1.33      1.17      1         0.833    ... ]                  normalized loading

Mission, AircraftLoading, WingLoading, ChordSparL, Beam |
                                  \bar{M}_{tip} : 1e-10                                                      Tip moment
                                  \bar{S}_{tip} : 1e-10                                                      Tip loading
                               \bar{\delta}_{root} : 1e-10                                                   Base deflection
                                  \theta_{root} : 1e-10                                                      Base angle

          Mission, AircraftLoading, WingLoading, GustL |
                                      N_{max} : 2                                                            max loading
                                    V_{gust} : 10                                      [m/s]                 gust velocity
                                       \kappa : 0.2                                                          max tip deflection ratio
                                \sigma_{CFRP} : 5.7e+08                                [Pa]                  CFRP max stress
                              \vec{1-cos(\eta)} : [ 1e-10     0.0761    0.293     0.617    ... ]             1 minus cosine factor

     Mission, AircraftLoading, WingLoading, GustL, Beam |
                                  \bar{M}_{tip} : 1e-10                                                      Tip moment
                                  \bar{S}_{tip} : 1e-10                                                      Tip loading
                               \bar{\delta}_{root} : 1e-10                                                   Base deflection
                                  \theta_{root} : 1e-10                                                      Base angle

       Mission, AircraftLoading, WingLoading, WingSkinL |
                                      C_{m_w} : 0.121                                                        negative wing moment coefficent
                                       V_{NE} : 45                                       [m/s]                 never exceed vehicle speed
                                     \rho_{sl} : 1.225                                   [kg/m**3]             air density at sea level
                                   \tau_{CFRP} : 570                                     [MPa]                 torsional stress limit

              Mission, FlightSegment, AircraftPerf |
                                      P_{acc} : 0                                        [W]                   Accessory power draw

        Mission, FlightSegment, AircraftPerf, WingAero |
                                            e : 0.9                                                          Oswald efficiency

             Mission, FlightSegment, FlightState |
                                   (E/S)_{irr} : 5716                                    [W*hr/m**2]           total daytime solar energy
                                   (E/S)_{var} : 1                                       [W*hr/m**2]           energy units variable
                                   (P/S)_{var} : 1                                       [W/m**2]              power units variable
                                 V_{wind-ref} : 100                                      [m/s]                 reference wind speed
                                           \mu : 1.42e-05                                [N*s/m**2]            viscosity
                                    \rho_{ref} : 1                                       [kg/m**3]             reference air density
                                       m_{fac} : 1                                                           wind speed margin factor
                                     p_{wind} : 0.9                                                          percentile wind speeds
                                     t_{night} : 13.78                                   [hr]                  Night span
```

```
Mission, FlightSegment, SteadyLevelFlight |
                        \eta_{prop} : 0.8                                                  propulsive efficiency

                               Wing |
                           \lambda : 0.5                                                   wing taper ratio
                            m_{fac} : 1.2                                                  wing weight margin factor
                 \vec{\bar{c}_{ave}} : [ 1.25      1.08      0.917     0.75     ]          normalized mid section chord
                       \vec{\bar{c}} : [ 1.33      1.17      1         0.833    ... ]      normalized chord at mid element

                     Wing, CapSpar |
                                 E : 2e+07                                  [psi]       Youngs modulus of CFRP
                       \rho_{CFRP} : 1.6                                    [g/cm**3]   density of CFRP
                                 g : 9.81                                   [m/s**2]    gravitational acceleration
                           w_{lim} : 0.15                                               spar width to chord ratio

                    Wing, WingSkin |
                          \bar{J/t} : 0.01114                               [1/mm]      torsional moment of inertia
                       \rho_{CFRP} : 1.6                                    [g/cm**3]   density of CFRP
                                 g : 9.81                                   [m/s**2]    gravitational acceleration
                           t_{min} : 0.012                                  [in]        minimum gague wing skin thickness
```

Sensitivities

```
                    Wing, WingSkin |
                                 g : 2.065                                  gravitational acceleration
                       \rho_{CFRP} : 2.065                                  density of CFRP
                           t_{min} : 2.065                                  minimum gague wing skin thickness

                     Wing, CapSpar |
                       \rho_{CFRP} : 0.3375                                 density of CFRP
                                 g : 0.3375                                 gravitational acceleration
                           w_{lim} : -0.0109                                spar width to chord ratio

                               Wing |
                            m_{fac} : 2.403                                 wing weight margin factor
                 \vec{\bar{c}_{ave}} : [ -0.167    -0.118    -0.0654   -0.0201  ]     normalized mid section chord

Mission, FlightSegment, SteadyLevelFlight |
                        \eta_{prop} : -6.582                                propulsive efficiency

     Mission, FlightSegment, FlightState |
                         t_{night} : 5.075                                  Night span
                          p_{wind} : 3.251                                  percentile wind speeds
```

\mu	2.133	viscosity
V_{wind-ref}	1.997	reference wind speed
m_{fac}	1.997	wind speed margin factor
(E/S)_{var}	1.259	energy units variable
(P/S)_{var}	-1.485	power units variable
(E/S)_{irr}	-2.544	total daytime solar energy
\rho_{ref}	-3.224	reference air density

Mission, FlightSegment, AircraftPerf, WingAero |

e	-2.952	Oswald efficiency

Mission, AircraftLoading, WingLoading, GustL |

N_{max}	0.3484	max loading
V_{gust}	0.2701	gust velocity
\vec{1-cos(\eta)}	[2.3e-12 0.00429 0.0364 0.125 ...]	1 minus cosine factor
\sigma_{CFRP}	-0.3484	CFRP max stress

Mission, AircraftLoading, EmpennageLoading, VerticalBoomTorsion |

\tau_{CFRP}	-0.1841	torsional stress limit

Mission, AircraftLoading, EmpennageLoading, VerticalBoomBending |

\theta_{max}	-0.6838	max tail boom deflection angle

Mission, AircraftLoading, EmpennageLoading, TailBoomState |

V_{NE}	1.736	never exceed vehicle speed
\rho_{sl}	0.868	air density at sea level

Mission, Aircraft, SolarCells |

g	0.4668	gravitational constant
\rho_{solar}	0.4668	solar cell area density
\eta	-2.771	Solar cell efficiency

Mission, Aircraft, Engine |

g	0.02216	gravitational constant
B_{PM}	-0.02216	power mass ratio

Mission, Aircraft, Empennage, VerticalTail |

V_v	1.995	vertical tail volume coefficient
C_{L_{max}}	0.868	maximum CL of vertical tail
m_{fac}	0.5917	vertical tail margin factor
\rho_{foam}	0.389	Density of formular 250
\bar{A}_{NACA0008}	0.389	cross sectional area of NACA 0008
g	0.2028	Gravitational acceleration
\rho_{skin}	0.2028	vertical tail skin density

\tau	0.1416	vertical tail thickness ratio
Mission, Aircraft, Empennage, TailBoom		
m_{fac}	0.868	tail boom margin factor
g	0.868	Gravitational acceleration
\rho_{CFRP}	0.868	density of CFRP
(1-k/2)	0.868	(1-k/2)
k	0.3039	tail boom inertia value
E	-0.6838	young's modulus carbon fiber
Mission, Aircraft, Empennage, HorizontalTail		
V_h	0.3254	horizontal tail volume coefficient
m_{fac}	0.1257	horizontal tail margin factor
\tau	0.09961	horizontal tail thickness ratio
g	0.07604	Gravitational acceleration
\rho_{skin}	0.07604	horizontal tail skin density
\rho_{foam}	0.04964	Density of formular 250
\bar{A}_{NACA0008}	0.04964	cross sectional area of NACA 0008
m_h	0.04723	horizontal tail span effectiveness
Mission, Aircraft, Empennage		
m_{fac}	1.585	Tail weight margin factor
Mission, Aircraft, Battery		
g	3.789	gravitational constant
\eta_{charge}	-1.583	Battery charging efficiency
h_{batt}	-3.789	battery energy density
\eta_{discharge}	-5.075	Battery discharging efficiency
Mission, Aircraft		
W_{pay}	0.7556	payload

A.2 Case 1: Hoburg Constraint Implemented as a Geometric Program

Cost

59.56 [lbf]

Free Variables

Mission, Aircraft |			
W_{cent} :	15.88	[lbf]	center weight
W_{total} :	59.56	[lbf]	aircraft weight
W_{wing} :	43.67	[lbf]	wing weight
Mission, Aircraft, Battery |			
E :	1.421e+07	[J]	total battery energy
W :	24.87	[lbf]	battery weight
\mathcal{V} :	0.03403	[m**3]	battery volume
Mission, Aircraft, Empennage |			
W :	5.743	[lbf]	empennage weight
Mission, Aircraft, Empennage, HorizontalTail |			
AR_h :	14.34		horizontal tail aspect ratio
C_{L_{max}} :	1.5		maximum CL of horizontal tail
S :	2.506	[ft**2]	horizontal tail area
W :	0.3715	[lbf]	horizontal tail weight
b :	5.994	[ft]	horizontal tail span
c_{r_h} :	0.4645	[ft]	horizontal tail root chord
c_{t_h} :	0.3716	[ft]	horizontal tail tip chord
l_h :	10.97	[ft]	horizontal tail moment arm
Mission, Aircraft, Empennage, TailBoom |			
I_0 :	6.813e-07	[m**4]	tail boom moment of inertia
J :	5.858e-07	[m**4]	tail boom polar moment of inertia
S :	13.76	[ft**2]	tail boom surface area
W :	2.607	[lbf]	tail boom weight
d_0 :	4.79	[in]	tail boom diameter
l :	10.97	[ft]	tail boom length
t_0 :	0.9633	[mm]	tail boom thickness
Mission, Aircraft, Empennage, VerticalTail |			
AR_v :	3.151		vertical tail aspect ratio
S :	10.14	[ft**2]	total vertical tail surface area
W :	2.765	[lbf]	one vertical tail weight
b :	5.653	[ft]	one vertical tail span
c_{r_v} :	2.11	[ft]	vertical tail root chord

```
                                                  c_{t_v} : 1.477                                  [ft]        vertical tail tip chord
                                                      l_v : 10.97                                  [ft]        horizontal tail moment arm

                                    Mission, Aircraft, Engine |
                                                  P_{max} : 265.2                                  [W]         max power
                                                        W : 0.1413                                 [lbf]       engine weight
                                                        m : 0.06405                                [kg]        engine mass

                                  Mission, Aircraft, SolarCells |
                                                        S : 55.39                                  [ft**2]     solar cell area
                                                        W : 3.064                                  [lbf]       solar cell weight

Mission, AircraftLoading, EmpennageLoading, HorizontalBoomBending |
                                                        F : 491.8                                  [N]         horizontal tail force
                                                  \theta : 0.06959                                             tail boom deflection angle

  Mission, AircraftLoading, EmpennageLoading, VerticalBoomBending |
                                                        F : 1016                                   [N]         vertical tail force
                                                  \theta : 0.1                                               tail boom deflection angle

  Mission, AircraftLoading, EmpennageLoading, VerticalBoomTorsion |
                                                        T : 1881                                   [N*m]       vertical tail moment

              Mission, AircraftLoading, WingLoading, ChordSparL |
                                             \vec{M_r} : [ 915       438       179       44.1     ]      [N*m]       wing section root moment

        Mission, AircraftLoading, WingLoading, ChordSparL, Beam |
                                                       dx : 0.25                                                       normalized length of element
                                           \vec{\bar{EI}} : [ 2.77      1.28      0.431     0.0599   ]              normalized YM and moment of inertia
                                            \vec{\bar{M}} : [ 0.677     0.324     0.133     0.0326   ... ]          normalized moment
                                            \vec{\bar{S}} : [ 1.49      0.839     0.474     0.205    ... ]          normalized shear
                                        \vec{\bar{\delta}} : [ 0.000376  0.0138    0.047     0.101    ... ]          normalized displacement
                                            \vec{\theta} : [ 0.000456  0.0548    0.117     0.199    ... ]          deflection slope

              Mission, AircraftLoading, WingLoading, GustL |
                                             \vec{M_r} : [ 1.25e+03  777       376       99.9     ]      [N*m]       wing section root moment
                                       \vec{\alpha_{gust}} : [ 7.85e-11  0.0274    0.1       0.205    ... ]          gust angle of attack
                                            \vec{\bar{q}} : [ 1.33      2.02      3.66      5.38     ... ]          normalized loading

            Mission, AircraftLoading, WingLoading, GustL, Beam |
                                                       dx : 0.25                                                       normalized length of element
                                           \vec{\bar{EI}} : [ 7.47      3.82      1.45      0.245    ]              normalized YM and moment of inertia
                                            \vec{\bar{M}} : [ 2.32      1.44      0.696     0.185    ... ]          normalized moment
                                            \vec{\bar{S}} : [ 3.74      3.32      2.61      1.48     ... ]          normalized shear
```

```
                \vec{\bar{\delta}} : [ 0.000209  0.0139    0.049     0.107    ... ]             normalized displacement
                    \vec{\theta} : [ 0.000403  0.0704    0.152     0.249    ... ]             deflection slope

    Mission, FlightSegment, AircraftPerf |
                             CDA : 0.004737                                                    non-wing drag coefficient
                             C_D : 0.02456                                                     aircraft drag coefficient
                        P_{oper} : 265.2                                          [W]          operating power
                       P_{shaft} : 0.3557                                         [hp]         shaft power

Mission, FlightSegment, AircraftPerf, TailAero |
                             C_d : 0.02361                                                     horizontal tail drag coefficient
                             C_d : 0.01009                                                     vertical tail drag coefficient
                              Re : 3.61e+04                                                    horizontal tail reynolds number
                              Re : 1.549e+05                                                   vertical tail reynolds number

Mission, FlightSegment, AircraftPerf, TailBoomAero |
                             C_f : 0.00733                                                     fuselage skin friction coefficient
                              Re : 9.472e+05                                                   fuselage reynolds number

Mission, FlightSegment, AircraftPerf, WingAero |
                             C_L : 0.886                                                       lift coefficient
                             C_d : 0.01982                                                     wing drag coefficient
                              Re : 9.523e+04                                                   Reynold's number
                          c_{dp} : 0.01372                                                     wing profile drag coeff

    Mission, FlightSegment, FlightState |
                         (E/S)_C : 193.2                                      [W*hr/m**2]      energy for batteries during sunrise/set
                     (E/S)_{day} : 2159                                       [W*hr/m**2]      solar cells energy during daytime
                     (P/S)_{min} : 234.3                                      [W/m**2]         minimum necessary solar power
                               V : 28.89                                      [m/s]            true airspeed
                       V_{wind} : 28.89                                       [m/s]            wind velocity
                            \rho : 0.1392                                     [kg/m**3]        air density

 Mission, FlightSegment, SteadyLevelFlight |
                               T : 7.344                                      [N]              thrust

                            Wing |
                              AR : 45.53                                                       aspect ratio
                               S : 55.39                                      [ft**2]          surface area
                               W : 15.74                                      [lbf]            weight
                            \tau : 0.2714                                                      airfoil thickness ratio
                               b : 50.21                                      [ft]             wing span
                           c_{MAC} : 1.103                                    [ft]             mean aerodynamic chord
                          c_{root} : 1.471                                    [ft]             root chord
```

```
                                \vec{c_{ave}} : [ 1.38      1.19      1.01      0.827    ]      [ft]        mid section chord

                                Wing, CapSpar |
                                            W : 1.193                                           [lbf]       spar weight
                                        \vec{I} : [ 2.5e-07   1.34e-07  5.5e-08   1.2e-08  ]      [m**4]      spar x moment of inertia
                                      \vec{S_y} : [ 2.2e-06   1.36e-06  6.6e-07   1.75e-07 ]      [m**3]      section modulus
                                       \vec{dm} : [ 0.12      0.0857    0.0489    0.0158   ]      [kg]        segment spar mass
                                   \vec{h_{in}} : [ 4.44      3.85      3.27      2.68     ]      [in]        inner spar height
                                        \vec{t} : [ 0.0245    0.0202    0.0136    0.00537  ]      [in]        spar cap thickness
                                        \vec{w} : [ 2.48      2.15      1.82      1.49     ]      [in]        spar width

                                Wing, WingSkin |
                                            W : 11.93                                           [lbf]       wing skin weight
                                            t : 0.012                                           [in]        wing skin thickness
```

Constants

```
                                Mission, Aircraft |
                                        W_{pay} : 10                                            [lbf]       payload

                            Mission, Aircraft, Battery |
                                  (E/\mathcal{V}) : 800                                         [W*hr/l]    volume battery energy density
                                    \eta_{charge} : 0.98                                                    Battery charging efficiency
                                 \eta_{discharge} : 0.98                                                    Battery discharging efficiency
                                               g : 9.81                                         [m/s**2]    gravitational constant
                                        h_{batt} : 350                                          [W*hr/kg]   battery energy density

                           Mission, Aircraft, Empennage |
                                       m_{fac} : 1                                                          Tail weight margin factor

       Mission, Aircraft, Empennage, HorizontalTail |
                                             V_h : 0.45                                                     horizontal tail volume coefficient
                                \bar{A}_{NACA0008} : 0.0548                                                 cross sectional area of NACA 0008
                                         \lambda : 0.8                                                      horizontal tail taper ratio
                            \lambda_h/(\lambda_h+1) : 0.4444                                                horizontal tail taper ratio factor
                                      \rho_{foam} : 1.5                                             [lbf/ft**3] Density of formular 250
                                      \rho_{skin} : 0.049                                           [g/cm**2]   horizontal tail skin density
                                            \tau : 0.08                                                     horizontal tail thickness ratio
                                               g : 9.81                                         [m/s**2]    Gravitational acceleration
                                             m_h : 5.514                                                    horizontal tail span effectiveness
                                           m_{fac} : 1.1                                                    horizontal tail margin factor

            Mission, Aircraft, Empennage, TailBoom |
                                       (1-k/2) : 0.6                                                        (1-k/2)
```

```
                                                E : 1.5e+11      [N/m**2]    young's modulus carbon fiber
                                        \rho_{CFRP} : 1.6        [g/cm**3]   density of CFRP
                                                g : 9.81         [m/s**2]    Gravitational acceleration
                                                k : 0.8                      tail boom inertia value
                                            m_{fac} : 1                      tail boom margin factor
                                            t_{min} : 0.25       [mm]        minimum tail boom thickness

                          Mission, Aircraft, Empennage, VerticalTail |
                                        C_{L_{max}} : 1.1                    maximum CL of vertical tail
                                                V_v : 0.04                   vertical tail volume coefficient
                                \bar{A}_{NACA0008} : 0.0548                  cross sectional area of NACA 0008
                                           \lambda : 0.7                     vertical tail taper ratio
                                \lambda_v/(\lambda_v+1) : 0.4118             vertical tail taper ratio factor
                                        \rho_{foam} : 1.5        [lbf/ft**3] Density of formular 250
                                        \rho_{skin} : 0.049      [g/cm**2]   vertical tail skin density
                                              \tau : 0.08                    vertical tail thickness ratio
                                                g : 9.81         [m/s**2]    Gravitational acceleration
                                            m_{fac} : 1.1                    vertical tail margin factor

                                    Mission, Aircraft, Engine |
                                         B_{PM} : 4141           [W/kg]      power mass ratio
                                                g : 9.81         [m/s**2]    gravitational constant

                                 Mission, Aircraft, SolarCells |
                                             \eta : 0.22                     Solar cell efficiency
                                        \rho_{solar} : 0.27      [kg/m**2]   solar cell area density
                                                g : 9.81         [m/s**2]    gravitational constant

Mission, AircraftLoading, EmpennageLoading, HorizontalBoomBending |
                                        \theta_{max} : 0.1                   max tail boom deflection angle

       Mission, AircraftLoading, EmpennageLoading, TailBoomState |
                                             V_{NE} : 40         [m/s]       never exceed vehicle speed
                                          \rho_{sl} : 1.225      [kg/m**3]   air density at sea level

  Mission, AircraftLoading, EmpennageLoading, VerticalBoomBending |
                                        \theta_{max} : 0.1                   max tail boom deflection angle

  Mission, AircraftLoading, EmpennageLoading, VerticalBoomTorsion |
                                        \tau_{CFRP} : 210        [MPa]       torsional stress limit

              Mission, AircraftLoading, WingLoading, ChordSparL |
                                         N_{max} : 5                         max loading
                                           \kappa : 0.2                      max tip deflection ratio
```

```
                                    \sigma_{CFRP} : 4.7e+08                                  [Pa]         CFRP max stress
                                    \vec{\bar{q}} : [ 1.33      1.17      1         0.833     ... ]                  normalized loading

Mission, AircraftLoading, WingLoading, ChordSparL, Beam |
                                    \bar{M}_{tip} : 1e-10                                                         Tip moment
                                    \bar{S}_{tip} : 1e-10                                                         Tip loading
                                \bar{\delta}_{root} : 1e-10                                                       Base deflection
                                    \theta_{root} : 1e-10                                                         Base angle

          Mission, AircraftLoading, WingLoading, GustL |
                                          N_{max} : 2                                                             max loading
                                          V_{gust} : 10                                  [m/s]                    gust velocity
                                            \kappa : 0.2                                                          max tip deflection ratio
                                    \sigma_{CFRP} : 5.7e+08                              [Pa]                     CFRP max stress
                                 \vec{1-cos(\eta)} : [ 1e-10     0.0761    0.293     0.617     ... ]              1 minus cosine factor

     Mission, AircraftLoading, WingLoading, GustL, Beam |
                                    \bar{M}_{tip} : 1e-10                                                         Tip moment
                                    \bar{S}_{tip} : 1e-10                                                         Tip loading
                                \bar{\delta}_{root} : 1e-10                                                       Base deflection
                                    \theta_{root} : 1e-10                                                         Base angle

       Mission, AircraftLoading, WingLoading, WingSkinL |
                                          C_{m_w} : 0.121                                                         negative wing moment coefficent
                                          V_{NE} : 45                                    [m/s]                    never exceed vehicle speed
                                        \rho_{sl} : 1.225                                [kg/m**3]                air density at sea level
                                    \tau_{CFRP} : 570                                    [MPa]                    torsional stress limit

                Mission, FlightSegment, AircraftPerf |
                                          P_{acc} : 0                                    [W]                      Accessory power draw

       Mission, FlightSegment, AircraftPerf, WingAero |
                                                e : 0.9                                                           Oswald efficiency

                Mission, FlightSegment, FlightState |
                                    (E/S)_{irr} : 5716                                   [W*hr/m**2]              total daytime solar energy
                                    (E/S)_{var} : 1                                      [W*hr/m**2]              energy units variable
                                    (P/S)_{var} : 1                                      [W/m**2]                 power units variable
                                  V_{wind-ref} : 100                                     [m/s]                    reference wind speed
                                            \mu : 1.42e-05                               [N*s/m**2]               viscosity
                                        \rho_{ref} : 1                                   [kg/m**3]                reference air density
                                          m_{fac} : 1                                                             wind speed margin factor
                                        p_{wind} : 0.9                                                            percentile wind speeds
                                        t_{night} : 13.78                                [hr]                     Night span
```

```
Mission, FlightSegment, SteadyLevelFlight |
                    \eta_{prop} : 0.8                                                  propulsive efficiency

                           Wing |
                      \lambda : 0.5                                                    wing taper ratio
                      m_{fac} : 1.2                                                    wing weight margin factor
  \vec{\bar{c}_{ave}} : [ 1.25      1.08      0.917     0.75     ]                    normalized mid section chord
        \vec{\bar{c}} : [ 1.33      1.17      1         0.833    ... ]                normalized chord at mid element

                 Wing, CapSpar |
                          E : 2e+07                                    [psi]         Youngs modulus of CFRP
                  \rho_{CFRP} : 1.6                                    [g/cm**3]     density of CFRP
                          g : 9.81                                     [m/s**2]      gravitational acceleration
                      w_{lim} : 0.15                                                   spar width to chord ratio

                Wing, WingSkin |
                     \bar{J/t} : 0.01114                               [1/mm]        torsional moment of inertia
                  \rho_{CFRP} : 1.6                                    [g/cm**3]     density of CFRP
                          g : 9.81                                     [m/s**2]      gravitational acceleration
                      t_{min} : 0.012                                  [in]          minimum gague wing skin thickness
```


Sensitivities

```
                Wing, WingSkin |
                          g : 1.23                                     gravitational acceleration
                  \rho_{CFRP} : 1.23                                   density of CFRP
                      t_{min} : 1.23                                   minimum gague wing skin thickness

                 Wing, CapSpar |
                  \rho_{CFRP} : 0.123                                  density of CFRP
                          g : 0.123                                    gravitational acceleration

                           Wing |
                      m_{fac} : 1.353                                  wing weight margin factor
  \vec{\bar{c}_{ave}} : [ -0.0574   -0.0409   -0.0231   -0.00731 ]     normalized mid section chord

Mission, FlightSegment, SteadyLevelFlight |
                    \eta_{prop} : -3.27                                propulsive efficiency

     Mission, FlightSegment, FlightState |
                     t_{night} : 2.604                                 Night span
                      p_{wind} : 1.407                                 percentile wind speeds
                  V_{wind-ref} : 0.9244                                reference wind speed
```

```
                                                m_{fac} : 0.9244                                    wind speed margin factor
                                                    \mu : 0.7567                                    viscosity
                                              (E/S)_{var} : 0.5285                                  energy units variable
                                              (P/S)_{var} : -0.6542                                 power units variable
                                              (E/S)_{irr} : -0.9949                                 total daytime solar energy
                                                \rho_{ref} : -1.501                                 reference air density

                        Mission, FlightSegment, AircraftPerf, WingAero |
                                                      e : -0.8121                                   Oswald efficiency

                          Mission, AircraftLoading, WingLoading, GustL |
                                                N_{max} : 0.1249                                    max loading
                                                V_{gust} : 0.09957                                  gust velocity
                                            \vec{1-cos(\eta)} : [ 9.95e-13  0.00158   0.0134    0.0462   ... ] 1 minus cosine factor
                                              \sigma_{CFRP} : -0.1249                               CFRP max stress

Mission, AircraftLoading, EmpennageLoading, VerticalBoomBending |
                                            \theta_{max} : -0.2275                                  max tail boom deflection angle

      Mission, AircraftLoading, EmpennageLoading, TailBoomState |
                                                V_{NE} : 0.455                                      never exceed vehicle speed
                                              \rho_{sl} : 0.2275                                    air density at sea level

                                 Mission, Aircraft, SolarCells |
                                                      g : 0.2633                                    gravitational constant
                                              \rho_{solar} : 0.2633                                 solar cell area density
                                                    \eta : -1.121                                   Solar cell efficiency

                                    Mission, Aircraft, Engine |
                                                      g : 0.01233                                   gravitational constant
                                                B_{PM} : -0.01233                                   power mass ratio

                          Mission, Aircraft, Empennage, VerticalTail |
                                                    V_v : 0.7149                                    vertical tail volume coefficient
                                                m_{fac} : 0.2413                                    vertical tail margin factor
                                              C_{L_{max}} : 0.2275                                  maximum CL of vertical tail
                                              \rho_{foam} : 0.1436                                  Density of formular 250
                                          \bar{A}_{NACA0008} : 0.1436                               cross sectional area of NACA 0008
                                                    \tau : 0.09925                                  vertical tail thickness ratio
                                                      g : 0.09775                                   Gravitational acceleration
                                              \rho_{skin} : 0.09775                                 vertical tail skin density

                       Mission, Aircraft, Empennage, TailBoom |
                                                m_{fac} : 0.2275                                    tail boom margin factor
```

g	0.2275	Gravitational acceleration
\rho_{CFRP}	0.2275	density of CFRP
(1-k/2)	0.2275	(1-k/2)
k	0.1011	tail boom inertia value
E	-0.2275	young's modulus carbon fiber
Mission, Aircraft, Empennage, HorizontalTail		
V_h	0.1373	horizontal tail volume coefficient
\tau	0.05737	horizontal tail thickness ratio
m_h	0.03736	horizontal tail span effectiveness
m_{fac}	0.03242	horizontal tail margin factor
g	0.02416	Gravitational acceleration
\rho_{skin}	0.02416	horizontal tail skin density
Mission, Aircraft, Empennage		
m_{fac}	0.5013	Tail weight margin factor
Mission, Aircraft, Battery		
g	2.137	gravitational constant
\eta_{charge}	-0.6192	Battery charging efficiency
h_{batt}	-2.137	battery energy density
\eta_{discharge}	-2.604	Battery discharging efficiency
Mission, Aircraft		
W_{pay}	0.8729	payload

A.3 Case 2: Hoburg Constraint Implemented as a Sequential Geometric Program

Cost

59.56 [lbf]

Free Variables

Mission, Aircraft |			
W_{cent} :	15.85	[lbf]	center weight
W_{total} :	59.56	[lbf]	aircraft weight
W_{wing} :	43.71	[lbf]	wing weight
Mission, Aircraft, Battery |			
E :	1.423e+07	[J]	total battery energy
W :	24.9	[lbf]	battery weight
\mathcal{V} :	0.03411	[m**3]	battery volume
Mission, Aircraft, Empennage |			
W :	5.711	[lbf]	empennage weight
Mission, Aircraft, Empennage, HorizontalTail |			
AR_h :	14.34		horizontal tail aspect ratio
C_{L_{max}} :	1.5		maximum CL of horizontal tail
S :	2.525	[ft**2]	horizontal tail area
W :	0.3747	[lbf]	horizontal tail weight
b :	6.017	[ft]	horizontal tail span
c_{r_h} :	0.4663	[ft]	horizontal tail root chord
c_{t_h} :	0.373	[ft]	horizontal tail tip chord
l_h :	10.98	[ft]	horizontal tail moment arm
Mission, Aircraft, Empennage, TailBoom |			
I_0 :	6.791e-07	[m**4]	tail boom moment of inertia
J :	5.857e-07	[m**4]	tail boom polar moment of inertia
S :	13.79	[ft**2]	tail boom surface area
W :	2.591	[lbf]	tail boom weight
d_0 :	4.799	[in]	tail boom diameter
l :	10.98	[ft]	tail boom length
t_0 :	0.9549	[mm]	tail boom thickness
Mission, Aircraft, Empennage, VerticalTail |			
AR_v :	3.157		vertical tail aspect ratio
S :	10.09	[ft**2]	total vertical tail surface area
W :	2.746	[lbf]	one vertical tail weight
b :	5.645	[ft]	one vertical tail span
c_{r_v} :	2.103	[ft]	vertical tail root chord

```
                                                  c_{t_v} : 1.472                                  [ft]        vertical tail tip chord
                                                      l_v : 10.98                                  [ft]        horizontal tail moment arm

                                        Mission, Aircraft, Engine |
                                                  P_{max} : 265.6                                  [W]         max power
                                                        W : 0.1415                                 [lbf]       engine weight
                                                        m : 0.06414                                [kg]        engine mass

                                      Mission, Aircraft, SolarCells |
                                                        S : 55.47                                  [ft**2]     solar cell area
                                                        W : 3.068                                  [lbf]       solar cell weight

Mission, AircraftLoading, EmpennageLoading, HorizontalBoomBending |
                                                        F : 493.5                                  [N]         horizontal tail force
                                                  \theta : 0.06988                                             tail boom deflection angle

  Mission, AircraftLoading, EmpennageLoading, VerticalBoomBending |
                                                        F : 1011                                   [N]         vertical tail force
                                                  \theta : 0.1                                               tail boom deflection angle

  Mission, AircraftLoading, EmpennageLoading, VerticalBoomTorsion |
                                                        T : 1873                                   [N*m]       vertical tail moment

                Mission, AircraftLoading, WingLoading, ChordSparL |
                                             \vec{M_r} : [ 903       429       175       43       ]      [N*m]       wing section root moment

          Mission, AircraftLoading, WingLoading, ChordSparL, Beam |
                                                       dx : 0.25                                                       normalized length of element
                                           \vec{\bar{EI}} : [ 2.79      1.28      0.416     0.0552   ]              normalized YM and moment of inertia
                                            \vec{\bar{M}} : [ 0.673     0.32      0.131     0.0321   ... ]          normalized moment
                                            \vec{\bar{S}} : [ 1.52      0.835     0.471     0.204    ... ]          normalized shear
                                        \vec{\bar{\delta}} : [ 0.000233  0.014     0.0468    0.1      ... ]          normalized displacement
                                             \vec{\theta} : [ 0.000458  0.054     0.115     0.197    ... ]          deflection slope

                  Mission, AircraftLoading, WingLoading, GustL |
                                             \vec{M_r} : [ 1.24e+03  771       374       99.2     ]      [N*m]       wing section root moment
                                       \vec{\alpha_{gust}} : [ 7.87e-11  0.0274    0.1       0.206    ... ]          gust angle of attack
                                            \vec{\bar{q}} : [ 1.33      2.02      3.66      5.38     ... ]          normalized loading

               Mission, AircraftLoading, WingLoading, GustL, Beam |
                                                       dx : 0.25                                                       normalized length of element
                                           \vec{\bar{EI}} : [ 7.59      3.89      1.46      0.235    ]              normalized YM and moment of inertia
                                            \vec{\bar{M}} : [ 2.32      1.44      0.696     0.185    ... ]          normalized moment
                                            \vec{\bar{S}} : [ 3.74      3.32      2.61      1.48     ... ]          normalized shear
```

```
                                \vec{\bar{\delta}} : [ 0.000228  0.014     0.0479    0.104    ... ]             normalized displacement
                                     \vec{\theta} : [ 0.000359  0.0687    0.148     0.242    ... ]             deflection slope

                    Mission, FlightSegment, AircraftPerf |
                                              CDA : 0.004741                                                   non-wing drag coefficient
                                              C_D : 0.02472                                                    aircraft drag coefficient
                                         P_{oper} : 265.6                                    [W]               operating power
                                        P_{shaft} : 0.3562                                   [hp]              shaft power

        Mission, FlightSegment, AircraftPerf, TailAero |
                                              C_d : 0.0236                                                     horizontal tail drag coefficient
                                              C_d : 0.01013                                                    vertical tail drag coefficient
                                               Re : 3.613e+04                                                  horizontal tail reynolds number
                                               Re : 1.539e+05                                                  vertical tail reynolds number

    Mission, FlightSegment, AircraftPerf, TailBoomAero |
                                              C_f : 0.007334                                                   fuselage skin friction coefficient
                                               Re : 9.452e+05                                                  fuselage reynolds number

        Mission, FlightSegment, AircraftPerf, WingAero |
                                              C_L : 0.8889                                                     lift coefficient
                                              C_d : 0.01998                                                    wing drag coefficient
                                               Re : 9.562e+04                                                  Reynold's number
                                            c_{dp} : 0.01376                                                   wing profile drag coeff

                    Mission, FlightSegment, FlightState |
                                          (E/S)_C : 193.2                                [W*hr/m**2]         energy for batteries during sunrise/set
                                       (E/S)_{day} : 2159                                [W*hr/m**2]         solar cells energy during daytime
                                       (P/S)_{min} : 234.3                               [W/m**2]            minimum necessary solar power
                                                 V : 28.84                               [m/s]               true airspeed
                                         V_{wind} : 28.84                                [m/s]               wind velocity
                                             \rho : 0.1391                               [kg/m**3]           air density

                 Mission, FlightSegment, SteadyLevelFlight |
                                                 T : 7.367                               [N]                 thrust

                                             Wing |
                                                AR : 44.96                                                   aspect ratio
                                                 S : 55.47                               [ft**2]             surface area
                                                 W : 15.73                               [lbf]               weight
                                              \tau : 0.27                                                    airfoil thickness ratio
                                                 b : 49.94                               [ft]                wing span
                                           c_{MAC} : 1.111                               [ft]                mean aerodynamic chord
                                          c_{root} : 1.481                               [ft]                root chord
```

```
                                \vec{c_{ave}} : [ 1.39      1.2       1.02      0.833    ]      [ft]        mid section chord

                                Wing, CapSpar |
                                            W : 1.176                                          [lbf]       spar weight
                                        \vec{I} : [ 2.48e-07  1.33e-07  5.47e-08  1.19e-08 ]      [m**4]      spar x moment of inertia
                                      \vec{S_y} : [ 2.18e-06  1.35e-06  6.55e-07  1.74e-07 ]      [m**3]      section modulus
                                       \vec{dm} : [ 0.118     0.0845    0.0482    0.0156   ]      [kg]        segment spar mass
                                    \vec{h_{in}} : [ 4.45      3.86      3.27      2.69     ]      [in]        inner spar height
                                        \vec{t} : [ 0.0241    0.0199    0.0134    0.00528  ]      [in]        spar cap thickness
                                        \vec{w} : [ 2.5       2.17      1.83      1.5      ]      [in]        spar width

                                Wing, WingSkin |
                                            W : 11.94                                          [lbf]       wing skin weight
                                            t : 0.012                                          [in]        wing skin thickness
```

Constants

```
                                Mission, Aircraft |
                                        W_{pay} : 10                                           [lbf]       payload

                            Mission, Aircraft, Battery |
                                  (E/\mathcal{V}) : 800                                        [W*hr/l]    volume battery energy density
                                    \eta_{charge} : 0.98                                                    Battery charging efficiency
                                 \eta_{discharge} : 0.98                                                    Battery discharging efficiency
                                               g : 9.81                                        [m/s**2]    gravitational constant
                                        h_{batt} : 350                                         [W*hr/kg]   battery energy density

                           Mission, Aircraft, Empennage |
                                       m_{fac} : 1                                                         Tail weight margin factor

                  Mission, Aircraft, Empennage, HorizontalTail |
                                           V_h : 0.45                                                    horizontal tail volume coefficient
                                \bar{A}_{NACA0008} : 0.0548                                              cross sectional area of NACA 0008
                                       \lambda : 0.8                                                     horizontal tail taper ratio
                          \lambda_h/(\lambda_h+1) : 0.4444                                               horizontal tail taper ratio factor
                                    \rho_{foam} : 1.5                                          [lbf/ft**3] Density of formular 250
                                    \rho_{skin} : 0.049                                        [g/cm**2]   horizontal tail skin density
                                          \tau : 0.08                                                     horizontal tail thickness ratio
                                             g : 9.81                                          [m/s**2]    Gravitational acceleration
                                           m_h : 5.514                                                   horizontal tail span effectiveness
                                       m_{fac} : 1.1                                                     horizontal tail margin factor

                       Mission, Aircraft, Empennage, TailBoom |
                                      (1-k/2) : 0.6                                                    (1-k/2)
```

```
                                                E : 1.5e+11      [N/m**2]    young's modulus carbon fiber
                                        \rho_{CFRP} : 1.6        [g/cm**3]   density of CFRP
                                                g : 9.81         [m/s**2]    Gravitational acceleration
                                                k : 0.8                      tail boom inertia value
                                            m_{fac} : 1                      tail boom margin factor
                                            t_{min} : 0.25       [mm]        minimum tail boom thickness

                                Mission, Aircraft, Empennage, VerticalTail |
                                        C_{L_{max}} : 1.1                    maximum CL of vertical tail
                                                V_v : 0.04                   vertical tail volume coefficient
                                \bar{A}_{NACA0008} : 0.0548                  cross sectional area of NACA 0008
                                           \lambda : 0.7                     vertical tail taper ratio
                                \lambda_v/(\lambda_v+1) : 0.4118             vertical tail taper ratio factor
                                        \rho_{foam} : 1.5        [lbf/ft**3] Density of formular 250
                                        \rho_{skin} : 0.049      [g/cm**2]   vertical tail skin density
                                              \tau : 0.08                    vertical tail thickness ratio
                                                g : 9.81         [m/s**2]    Gravitational acceleration
                                            m_{fac} : 1.1                    vertical tail margin factor

                                        Mission, Aircraft, Engine |
                                            B_{PM} : 4141        [W/kg]      power mass ratio
                                                g : 9.81         [m/s**2]    gravitational constant

                                    Mission, Aircraft, SolarCells |
                                              \eta : 0.22                    Solar cell efficiency
                                        \rho_{solar} : 0.27      [kg/m**2]   solar cell area density
                                                g : 9.81         [m/s**2]    gravitational constant

Mission, AircraftLoading, EmpennageLoading, HorizontalBoomBending |
                                        \theta_{max} : 0.1                   max tail boom deflection angle

       Mission, AircraftLoading, EmpennageLoading, TailBoomState |
                                            V_{NE} : 40          [m/s]       never exceed vehicle speed
                                          \rho_{sl} : 1.225      [kg/m**3]   air density at sea level

  Mission, AircraftLoading, EmpennageLoading, VerticalBoomBending |
                                        \theta_{max} : 0.1                   max tail boom deflection angle

  Mission, AircraftLoading, EmpennageLoading, VerticalBoomTorsion |
                                        \tau_{CFRP} : 210        [MPa]       torsional stress limit

              Mission, AircraftLoading, WingLoading, ChordSparL |
                                            N_{max} : 5                      max loading
                                             \kappa : 0.2                    max tip deflection ratio
```

```
                                \sigma_{CFRP} : 4.7e+08                                    [Pa]         CFRP max stress
                                \vec{\bar{q}} : [ 1.33      1.17      1         0.833     ... ]                  normalized loading

Mission, AircraftLoading, WingLoading, ChordSparL, Beam |
                                  \bar{M}_{tip} : 1e-10                                                       Tip moment
                                  \bar{S}_{tip} : 1e-10                                                       Tip loading
                               \bar{\delta}_{root} : 1e-10                                                    Base deflection
                                  \theta_{root} : 1e-10                                                       Base angle

          Mission, AircraftLoading, WingLoading, GustL |
                                      N_{max} : 2                                                             max loading
                                      V_{gust} : 10                                          [m/s]            gust velocity
                                        \kappa : 0.2                                                          max tip deflection ratio
                                    \sigma_{CFRP} : 5.7e+08                                  [Pa]             CFRP max stress
                                \vec{1-cos(\eta)} : [ 1e-10     0.0761    0.293     0.617     ... ]           1 minus cosine factor

     Mission, AircraftLoading, WingLoading, GustL, Beam |
                                  \bar{M}_{tip} : 1e-10                                                       Tip moment
                                  \bar{S}_{tip} : 1e-10                                                       Tip loading
                               \bar{\delta}_{root} : 1e-10                                                    Base deflection
                                  \theta_{root} : 1e-10                                                       Base angle

       Mission, AircraftLoading, WingLoading, WingSkinL |
                                      C_{m_w} : 0.121                                                         negative wing moment coefficent
                                       V_{NE} : 45                                           [m/s]            never exceed vehicle speed
                                     \rho_{sl} : 1.225                                       [kg/m**3]        air density at sea level
                                   \tau_{CFRP} : 570                                         [MPa]            torsional stress limit

             Mission, FlightSegment, AircraftPerf |
                                      P_{acc} : 0                                           [W]              Accessory power draw

       Mission, FlightSegment, AircraftPerf, WingAero |
                                            e : 0.9                                                           Oswald efficiency

             Mission, FlightSegment, FlightState |
                                   (E/S)_{irr} : 5716                                       [W*hr/m**2]      total daytime solar energy
                                   (E/S)_{var} : 1                                          [W*hr/m**2]      energy units variable
                                   (P/S)_{var} : 1                                          [W/m**2]         power units variable
                                 V_{wind-ref} : 100                                         [m/s]            reference wind speed
                                           \mu : 1.42e-05                                   [N*s/m**2]       viscosity
                                     \rho_{ref} : 1                                         [kg/m**3]        reference air density
                                        m_{fac} : 1                                                          wind speed margin factor
                                      p_{wind} : 0.9                                                         percentile wind speeds
                                     t_{night} : 13.78                                      [hr]             Night span
```

```
Mission, FlightSegment, SteadyLevelFlight |
                    \eta_{prop} : 0.8                                                  propulsive efficiency

                           Wing |
                      \lambda : 0.5                                                    wing taper ratio
                       m_{fac} : 1.2                                                   wing weight margin factor
          \vec{\bar{c}_{ave}} : [ 1.25      1.08      0.917     0.75     ]            normalized mid section chord
                \vec{\bar{c}} : [ 1.33      1.17      1         0.833    ... ]        normalized chord at mid element

                 Wing, CapSpar |
                          E : 2e+07                                  [psi]       Youngs modulus of CFRP
                \rho_{CFRP} : 1.6                                    [g/cm**3]   density of CFRP
                          g : 9.81                                   [m/s**2]    gravitational acceleration
                      w_{lim} : 0.15                                             spar width to chord ratio

                Wing, WingSkin |
                     \bar{J/t} : 0.01114                           [1/mm]      torsional moment of inertia
                \rho_{CFRP} : 1.6                                    [g/cm**3]   density of CFRP
                          g : 9.81                                   [m/s**2]    gravitational acceleration
                      t_{min} : 0.012                                [in]        minimum gague wing skin thickness
```


Sensitivities

```
                Wing, WingSkin |
                          g : 1.209                                  gravitational acceleration
                \rho_{CFRP} : 1.209                                  density of CFRP
                      t_{min} : 1.209                                minimum gague wing skin thickness

                 Wing, CapSpar |
                \rho_{CFRP} : 0.119                                  density of CFRP
                          g : 0.119                                  gravitational acceleration

                           Wing |
                       m_{fac} : 1.328                               wing weight margin factor
          \vec{\bar{c}_{ave}} : [ -0.0554   -0.0395   -0.0223   -0.00707 ]          normalized mid section chord

Mission, FlightSegment, SteadyLevelFlight |
                    \eta_{prop} : -3.213                             propulsive efficiency

     Mission, FlightSegment, FlightState |
                     t_{night} : 2.558                               Night span
                      p_{wind} : 1.396                               percentile wind speeds
                   V_{wind-ref} : 0.9161                             reference wind speed
```

```
                                                m_{fac} : 0.9161                                    wind speed margin factor
                                                    \mu : 0.7754                                    viscosity
                                              (E/S)_{var} : 0.5186                                  energy units variable
                                              (P/S)_{var} : -0.6422                                 power units variable
                                              (E/S)_{irr} : -0.9757                                 total daytime solar energy
                                                \rho_{ref} : -1.488                                 reference air density

                      Mission, FlightSegment, AircraftPerf, WingAero |
                                                      e : -0.8079                                   Oswald efficiency

                        Mission, AircraftLoading, WingLoading, GustL |
                                                N_{max} : 0.1208                                    max loading
                                              V_{gust} : 0.09631                                    gust velocity
                                          \vec{1-cos(\eta)} : [ -5.33e-12  0.00152   0.0129    0.0447   ... ] 1 minus cosine factor
                                             \sigma_{CFRP} : -0.1208                                CFRP max stress

Mission, AircraftLoading, EmpennageLoading, VerticalBoomBending |
                                             \theta_{max} : -0.222                                  max tail boom deflection angle

      Mission, AircraftLoading, EmpennageLoading, TailBoomState |
                                                V_{NE} : 0.444                                      never exceed vehicle speed
                                              \rho_{sl} : 0.222                                     air density at sea level

                               Mission, Aircraft, SolarCells |
                                                      g : 0.2589                                    gravitational constant
                                            \rho_{solar} : 0.2589                                   solar cell area density
                                                    \eta : -1.099                                   Solar cell efficiency

                                  Mission, Aircraft, Engine |
                                                      g : 0.01212                                   gravitational constant
                                              B_{PM} : -0.01212                                     power mass ratio

                          Mission, Aircraft, Empennage, VerticalTail |
                                                    V_v : 0.6968                                    vertical tail volume coefficient
                                              m_{fac} : 0.2353                                      vertical tail margin factor
                                            C_{L_{max}} : 0.222                                     maximum CL of vertical tail
                                            \rho_{foam} : 0.1398                                    Density of formular 250
                                         \bar{A}_{NACA0008} : 0.1398                                cross sectional area of NACA 0008
                                                  \tau : 0.09662                                    vertical tail thickness ratio
                                                      g : 0.09549                                   Gravitational acceleration
                                            \rho_{skin} : 0.09549                                   vertical tail skin density

                             Mission, Aircraft, Empennage, TailBoom |
                                              m_{fac} : 0.222                                       tail boom margin factor
```

g	0.222	Gravitational acceleration
\rho_{CFRP}	0.222	density of CFRP
(1-k/2)	0.222	(1-k/2)
k	0.09866	tail boom inertia value
E	-0.222	young's modulus carbon fiber
Mission, Aircraft, Empennage, HorizontalTail		
V_h	0.1351	horizontal tail volume coefficient
\tau	0.05632	horizontal tail thickness ratio
m_h	0.03663	horizontal tail span effectiveness
m_{fac}	0.0321	horizontal tail margin factor
g	0.02389	Gravitational acceleration
\rho_{skin}	0.02389	horizontal tail skin density
Mission, Aircraft, Empennage		
m_{fac}	0.4893	Tail weight margin factor
Mission, Aircraft, Battery		
g	2.101	gravitational constant
\eta_{charge}	-0.6072	Battery charging efficiency
h_{batt}	-2.101	battery energy density
\eta_{discharge}	-2.558	Battery discharging efficiency
Mission, Aircraft		
W_{pay}	0.8568	payload